Neural Tube Defect-causing Teratogens Affect Tissue Mechanical Properties and Cytoskeletal Morphology in Axolotl Embryos

by

Fatima Kakal

A thesis
presented to the University of Waterloo
in fulfillment of the
thesis requirement for the degree of
Master of Science
in
Biology

Waterloo, Ontario, Canada, 2007

AUTHOR'S DECLARATION

I hereby declare that I am the sole author of this thesis. This is a true copy of the thesis, including any required final revisions, as accepted by my examiners.

I understand that my thesis may be made electronically available to the public.

Abstract

The teratogenic drugs cytochalasin B and valproic acid have been shown to alter F-actin polymerization, an effect that is crucial in forming microfilaments. Microfilaments form important cytoskeletal structures that maintain the structural integrity of the cell, cause cell motility and cell migration. Microfilament alterations are known to cause neural tube defects such as spina bifida and anencephaly (Walmod et al., 1999). We here aim to show that disruption of microfilaments by cytochalasin B and valproic acid affects the tensile properties of the tissue. Biomechanics is an interdisciplinary field that allows mechanical concepts to help us understand embryo development. This project used a novel tissue stretching device that measures the tensile properties of neural and epidermal tissue. The instrument used a pair of cantilevered wires to which the specimen was glued. This device stretched the mid-neural and -lateral tissue anterior-posterior (AP) and medio-lateral (ML) unidirectionally. The tensile properties of the tissue were determined by Resultant Young's Modulus that depends on the true stress and true strain in the tissue sample. The experiment was conducted at a strain rate of 50%. Axolotl embryos were treated with 5ug/mL and 2.5ug/mL cytochalasin B and 5mM valproic acid at stage 13 (early neurula) for an hour, washed, and allowed to develop to stage 15 before it was used in the uniaxial tissue stretcher. Changes in the F-actin filaments were analysed by phalloidin staining and viewed under a confocal microscope. The tests show that disruption of microfilaments by cytochalasin B increases the stiffness of the dorsal-tissue by as much as 101% for CB-treated tissues stretched in the AP direction and 298% when stretched in the ML direction. VA-treated neural plate tissue showed a stiffness increase of 278% when stretched in the AP direction and 319%, when stretched in the ML direction. Changes in the F-actin filaments are quantified by phalloidin staining viewed with confocal microscopy. These findings indicate that direction-dependent mechanical forces in the tissue are contributing factors in closure of the neural tube in axolotl embryos.

Acknowledgements

I would like to thank Dr. Brodland for mentorship and advice and Dr. Marsden for our long conversations on embryo development. Furthermore I would like to thank Jim Veldhius for writing the software and Caleb Horst for helping me with data analysis and exhibiting extreme patience. Additionally, I would like to thank Colin Wiebe and Richard Benko for teaching me how to use the tissue stretcher. Lastly, I would like to thank Jennifer Sweny for phalloidin staining.

I would like to thank Abby Li for her friendship, for always being there, for always understanding and for always caring.

I would like to acknowledge the support I received from my husband Mustafa, who I deeply respect and will forever love; and my parents, their prayers making it possible for me to reach this far.

Lastly, I would like to thank all the great people that I met during this journey, Dr. Ranjana Bird, Hussain Kakal & Rose Vogt, to name a few. Their words of encouragement and faith in my work allowed me to attain this goal.

Dedication

To Mustafa, I love you!

In the name of Allah, the Most Merciful and the Most Beneficial

Table of Contents

List of Tables

List of Figures

Chapter 1: Introduction

1.1 Objective

The process by which the neural tube forms has intrigued scientists for hundreds of years. Biochemical analyses, molecular genetics, 3-D image reconstruction, biomechanics, developmental phenotyping and computer modeling have shown that neurulation is a multi-faceted process (Clausi and Brodland, 1993; Schoenwolf and Smith, 1990 & Gordon, 1985). In order to better understand the biomechanics of neurulation, this project uses a novel tissue stretching device that measures the tensile properties of normal and drug-treated neural and epidermal tissue and confocal microscopy to relate mechanical property changes to cytoskeletal alterations. Biomechanics is an interdisciplinary field that allows mechanical concepts to help us understand embryo development.

Mechanical property data are important for understanding how embryonic tissues interact with each other during early embryo morphogenesis. It provides for mechanical quantification of cytoskeletal structures such as actin and tubulin as well as determines the contributions of membrane proteins by selectively removing these proteins and testing the tensile properties change of the tissue. The force in the tissue as it stretches is used to calculate the engineering stress. The degree of stretching determines the engineering strain. The ratio of the two values provides the Young's Modulus. Once the Young's Modulus of the neural and lateral epithelium from various regions and stages of the neurulating embryo is determined, the values can then be used to construct 3-D models of embryonic movements.

By using teratogens that target specific proteins of interest, we hope to determine the correlation between cytoskeletal characteristics and tissue properties. Cytochalasin B, a known inhibitor of actin polymerization was used Valproic Acid, a known inducer of actin polymerization was also used. Control tissue and teratogen-treated tissue were then tested to determine their mechanical properties. In this study, tissues from fifty-one embryos were stretched along the anterior-posterior or medio-lateral axes. The regions under study were the mid-dorsal, neural epithelium and mid-lateral epidermal tissue of stage 15 embryos. Control embryos were used as a comparison to

deduce the effect of cytochalasin B and valproic acid on cytoskeletal morphology, tissue properties and embryo development.

1.2 Why Study Axolotls?

The model organism used for this project is the Mexican Salamander (*Ambystoma mexicanum*) or axolotl. One reason is that their development can be controlled by the external temperature (lower temperatures slow development) so that individual embryos in a batch can be time shifted with respect to each other to facilitate the sequential study of successive embryos. Secondly axolotl embryos have large cells allowing for easy micromanipulations. The intricate act of gluing cantilever wires on the neural plate to determine the mechanical properties is only possible on large embryos like axolotls. Furthermore cells have natural pigmentation thus allowing easy visualization of cell shape changes and staining. Variegation in egg pigmentation provides built-in markers for the tracking of individual cells. The pigmentation further allows differentiation between the neural anlage and epidermal layer. Also, the neural tube is a monolayer just like it is in humans. Last but not the least, intensive research on understanding the mechanisms of neurulation has been previously performed on axolotl embryos, thereby providing a large knowledge base.

1.3 Stages of Axolotl Development

In axolotl embryos, the process of neurulation starts at stage 13 and continues to stage 20. In *Xenopus* the induction of neural fate in the target ectoderm during gastrulation depends on complex tissue interaction and extracellular signals from the dorsal chordamesoderm (Spemann's Organizer) (Nieuwkoop et al., 1985). This pre-patterning then allows for massive cell movements and tissue changes that are part of neurulation. The process of neurulation in axolotl begins with the initial formation of the neural cleft and continues with the final closure of the neural plate to form a neural tube. This process is illustrated in Figure 1.1 by Bordzilovskaya *et al.* (1989). The crucial moment for the neurulating embryo is stage 15 where the neural plate is completely exposed right before closure. Experimental analysis to determine the structural integrity and tissue mechanics was conducted at stage 15.

13. Early neurula I, vegetal hemisphere

13. Early neurula I, side view

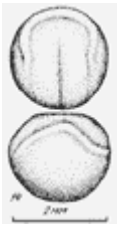

14. Early neurula II

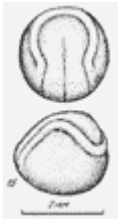

15. Early neurula III

16. Middle neurula II

17. Late neurula I

18. Late neurula II

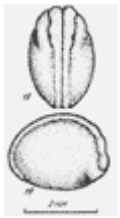

19. Late neurula III

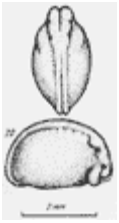

20. Late neurula IV

Figure 1.1 Stages of embryo development (Bordzilovskaya et al., 1989)

1.4 Neurulation

Neurulation is the process by which the neural plate rolls up to form the neural tube, and it is the third process of embryonic development, after blastulation and gastrulation. The neural tube is the precursor of the central nervous system and is established during this multifaceted process (Schoenwolf and Smith, 1990). Neural tube formation is a highly regulated and coordinated process orchestrated by a number of biochemical pathways and mechanical forces (Clausi and Brodland, 1993). This complex procedure is divided into many sub-processes, some that are interlinked and interdependent while others occur in differently induced conditions. Neural plate closure is autonomous and cell shape changes are important in neural plate formation (Burns and Garson, 1983). Anomalies during neurulation can result in neural tube defects.

The neural tube is formed by primary neurulation and in some species followed by secondary neurulation. Primary neurulation is triggered by the surrounding cells and results in the rolling of a flat neural plate to fuse towards the centre midline to form the neural tube. During primary neurulation, the ectoderm is divided into three important sections: The internally-positioned neural plate cells, which will form the brain and the spinal cord; the mid-neural crest cells, that will migrate to form the mesenchyme; and lastly the externally-positioned epidermis, which will fuse over the neural tube as it internalizes, to form the skin. The process of primary neurulation appears to be similar in amphibians, reptiles, birds, fish and mammals with a few subtle differences (Gallera, 1971). Secondary neurulation arises from a solid cord of cells that sinks into the embryo and cavitates to form a hollow tube. In amphibians, most of the tadpole neural tube forms by primary neurulation, while the tail forms by secondary neurulation (Gont et. al., 1993).

1.4.1 Mechanism of Neural Tube Formation

Neurulation is the process by which the presumptive neural tissue converges and extends to form the neural tube and the neural crest cells.

1.4.1.1 Convergent Extension

The process by which cells intercalate and extend to convert a ball of cells into an elongated adult, without significant cell division, is called convergent extension. Convergent extension is triggered by cell shape changes and cell movements. Prior to the onset of neurulation, the presumptive neural ectoderm of the newt consists of a low columnar epithelium, the same morphology as the non-neural ectoderm (Karfunkel, 1974). Burnside (1973) concluded that there are three major cell shape changes of the salamander ectoderm as it undergoes neurulation. Post-gastrulation the ectodermal cells are uniform and indistinguishable from one another. The first event of neurulation is the dramatic elongation of all the cells in the presumptive neural plate. This causes the embryo to experience a wave formation in the overlying ectoderm indicating the initiation of the neural induction process (Brodland et. al., 1994). After the cells elongate, there is sequential constriction of the cell apices, beginning with cells near the neural fold (Karfunkel, 1974; Burnside 1973), and an increase in thickness by about three fold (Jacobson, 1991). The presumptive neural tissue of *Taricha torosa* is two cells thick. On the other hand the presumptive uni-layered epidermal cells flatten throughout neurulation and eventually form the squamous epithelium (Burnside, 1973). The process of cell elongation and apical constriction require microtubule and microfilaments respectively. The neural plate undergoes convergent extension mostly by the process of lateral intercalation, illustrated in Figure 1.2B. Mediolateral intercalation of mesodermal cells is driven by mediolaterally polarized protrusive activity (Keller, 2002) illustrated by Figure 1.2A. However intercalation of more lateral cells in the posterior neural plate involves medially oriented monopolar protrusions, whereas the more medial cells of the notoplate display randomly oriented motility (Wallingford and Harland, 2001). During intercalation, medial and mediolaterally protruding lamellipodia attach to and crawl on adjacent cells. As a result of this traction, cells elongate and intercalate along the mediolateral axis to form a longer narrower array. Furthermore cell division takes place in the anterior-posterior direction. When posterior neural tissue is cultured in isolation, neural cells will intercalate using bipolar mediolaterally oriented lamellapodia (Figure 1.2C). Isolated cells become longer and narrower but fail to roll up into a neural tube implying that intrinsic forces are contributing factors to neural convergent extension but extrinsic forces are required for neural tube development.

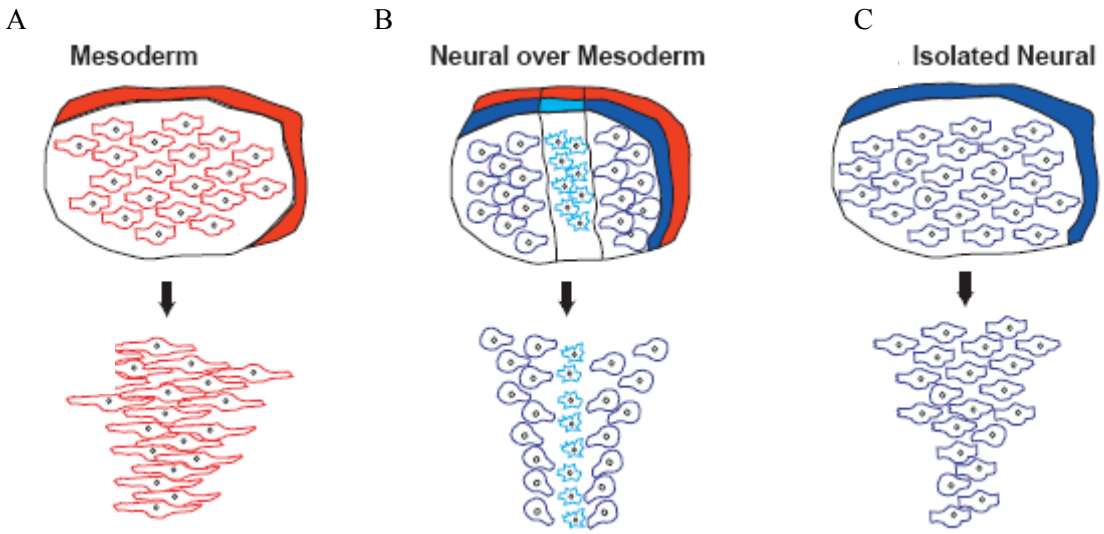

Figure 1.2 A. Cells undergoing mediolateral intercalation in the mesoderm. B. Medially oriented protrusions in the more lateral neural plate over mesoderm. C. Mediolateral intercalation in isolated posterior neural ectoderm. (Red; mesoderm, blue; neural ectoderm, light-blue; notocord (Wallingford and Harland, 2001).

1.4.1.2 Neural Plate Formation

The first visible feature of the future neural plate appears at stage 12 by the formation of a dorsal median groove (Neiwkoop, 1999), starting at the blastopore to the center of the presumptive neural plate. At stage 13 of *Xenopus* neurulation, the median groove corresponds to the position of the underlying notochordal anlage and point of archentron roof attachment and underlying ectoderm (Niewkoop, 1999). Cells at the midline of the neural plate are called median hinge point (MHP) cells and are anchored to the notochord beneath. These form a hinge which forms a furrow at the dorsal midline. The notochord induces the MHP cells to decrease their height and become wedged-shaped. Two more hinges form at the intersection of the neural plate and epidermis. These are called the dorsolateral hinge points (DLHP), and are anchored to the surface ectoderm of the neural folds. These cells increase their heights and become wedged-shape. However in axolotls, the notochord starts to form after the neural tube closure (Burn and Garson 1984). Therefore it is important to understand the mechanisms that cause the first furrow formation in the marginal hinge point in axolotl. The hinges form pivots that direct the rotation of cells along it.

Cells in the lateral neural plate form bottle-shaped structures by cell wedging, allowing them to invaginate along the neural plate boundary. Cell wedging is caused by actin polymerization

resulting in apical constriction (Brun and Garson 1984). Burnside (1973) found a strong correlation between the apical surface area changes and total surface area changes of individual cells at a specific region of the neural plate in newt embryos. Since the cell volume remained constant, the cell shape must change by lengthening and narrowing. Thus the change in surface area of a cell is directly related to the degree of elongation of the cell (Burnside 1973).

1.4.1.3 Neural Tube Formation

The neural plate rolls up in order to form the neural tube. After neural plate formation, the lateral edges thicken and move upwards to form the neural ridge forming a U-shaped neural groove in the center of the plate. At stage 14 the outer boundary of the neural plate becomes visible by neural fold elevation (Niewkoop, 1999). The neural plate changes from a visible horseshoe shape to a more keyhole shape by the extension of the posterior region (Burnside and Jacobson, 1968). The anterior portion of the neural plate reaches its maximum width at stage 15, at which the neural folds migrate towards the midline of the embryo and fuse together to form the neural tube. The lateral neural folds approach and make contact with each other in the future hindbrain region. Neural tube closure does not occur simultaneously along the tube. It starts at the mid-dorsal region and zips-up in both directions, first towards the posterior end followed by the anterior end. The complete fusion of the neural plate occurs at tail bud stage, 20/21. The cells at the ridge, the neural crest cells, migrate to other regions of the developing embryo and become precursor cells to other organs.

1.4.2 Mechanical Forces that Drive Neurulation

Neural tube formation can be a cumulative affect of forces potentially arising from various parts of the embryo. The exact mechanism of the neural tube formation is not known. Some say forces in the lateral epithelial and ventral regions can render the closure of the neural plate to be a passive event (Karfunkel, 1974). Others feel intrinsic forces within the neural plate caused by apical constriction of the cell can further promote the neural ridges to close (Burnside, 1973). Still other scientists proclaim forces in the chordamesoderm under the neural anlage can trigger this process (Shroeder, 1970). According to Gilbert, (2003) closure of the neural tube requires extrinsic forces that push towards the midline and allows the neural tube to invaginate inside the dorsal surface of the embryo. . The relative importance of these mechanisms may be species specific. Computer models have provided important

insights into the mechanics of neurulation (Brodland, 2003). This section reviews the various mechanical forces that perhaps drive neurulation.

1.4.2.1 Non-Neural Ectoderm

Many schools of thought attribute the closure of the neural tube to forces from the non-neural ectoderm (Karfunkel, 1974; Burnside, 1973). During the neural plate stage both the neural and non-neural ectoderm have a high mitotic index compared to the neural groove stage. Karfunkel, (1974) concluded that neurulation might be brought about by a growth of recently-formed daughter cells within the non-neural ectoderm. This theory was for the first time proposed by His (1874), who suggested that the epidermis surrounding the neural plate expands, pushing the neural plate into a tube (Jacobson, 1991). However in 1888 Roux refuted this theory by separating the neural plate from the epidermis to reveal that the plate forms a tube faster than in whole embryos. Roux (1888) suggested that rather than aiding the neural tube formation, the epidermis hinders the process. The epidermis is under tension and if the neural plate is excised from the embryo during neurulation, it immediately contracts towards the midline (Jacobson, 1991). In conclusion, the epidermis has a role in organizing pulling forces as opposed to pushing the neural anlage into forming a tube.

1.4.2.2 Neural Ridges

Micromanipulation of the neural plate suggests the neural ridges might also play an important role. Embryos with laterally excised tissue continue to neurulate in the presence of neural ridges and neural plate. The first experiment to demonstrate the autonomous nature of neural tissue was performed by Jacobson (1962), in which the neural plate was excised from the epidermal and mesodermal cells and was able to fold independently. In 1974 Karfunkel repeated those experiments and attributed the medial migration of the neural folds after the neural plate is removed to the wound healing process. It is also important to note that neural closure depends on the stage of the embryo undergoing surgery. If the lateral tissue is excised before the fate of the neural plate has been determined, then the neural tube does not form.

1.4.2.3 Intrinsic Forces

Compelling evidence by Burnside (1973) suggests that the shape of the cells in the neural plate provide intrinsic forces that allow neurulation. Burnside (1973) observed that isolated salamander

neural plate cells continue to elongate and retain their columnar shape in culture in the absence of surrounding tissue. This shows the capacity to elongate is intrinsic to the cells and does not represent a passive accommodation of external forces. Furthermore the apical constriction of neural plate cells has been identified as a contributing force in neurulation (Jacobson, 1991).

1.4.2.4 Chordamesoderm

The mesoderm cells located beneath the neural plate, along with the notochord, are known as the chordamesoderm. Even though Burnside's (1973) experiment allowed the neural plate to close in the absence of a substrate that may provide mechanical force, several scientists have suggested the possibility that proliferation of the mesoderm lying under the neural plate might cause the elevation of the neural folds (Karfunkel, 1974). In *Xenopus* the elevation of the neural folds seems to be enhanced by the thickening of the mesoderm found to lie immediately beneath the folds. Shroeder (1970) noted the possibility that myotome proliferation might act to effect neurulation. However, no such mechanism has been seen in axolotls. On the contrary the axolotl neural plate is loosely attached to the underlying mesoderm and can easily be separated, thus diminishing the possibility of a role for the chordomesoderm in providing underlying forces. In another series of experiments, Burnside (1972) isolated the neural plate from *Ambystoma* embryos of various stages leaving the subjacent mesoderm cells under one-half and removing these cells from the other half. When the neural plate is excised from stage 12 to stage 14 embryos, the half that retains the mesodermal cells do not curl up, but the half that does not have the mesodermal cells immediately curl up in the opposite direction. Wound-healing process can be attributed to curling of the neural plate. However, in that case, both the ends would curl in the opposite direction. Furthermore the notochord, which appears to play a vital role in *Xenopus*, develops after neural tube closure in axolotls. It is safe to conclude that there are strong evidences for and against the chordamesoderm providing mechanical forces in the tissue. The above section summarises the sources of mechanical forces in the embryo that may drive the process of neurulation. However, not many people have physically measured these forces in a stringent manner that would allow us to quantify the process of neurulation.

1.4.3 Mesodermal Induction and Ectodermal Competence

Induction and competence are important aspects that drive the process of neurulation. The ability of the ectoderm to respond to the underlying mesoderm signalling is known as competence. The neural fate is determined by complex signalling from the dorsal chordamesoderm (Spemann's Organizer) to the ectoderm above it (Gilbert 2003). The dorsal ectoderm exhibits competence which allows the Spemann's Organizer to induce neural plate formation. Signalling membrane proteins in the neural ectoderm have been characterized as crucial elements in rendering the ectoderm competent. Recent advances have been made in the identification of molecules involved in the patterning of the neural plate. The neural tube separates from the epidermis due to expression of different cell adhesion molecules. Initially the ectoderm contains E-cadherin that is normally found in the epidermis. During the onset of neural tube formation, cells in the neural plate stop producing E-cadherins and instead produce N-cadherins and N-calmodulins; this results in differential adhesion between the surface ectoderm and neural plate tissue. Ectopic expression of N-cadherin in the ectoderm severely impedes neural tube formation (Gilbert, 2003). Expression of different cell adhesion molecules triggers the ectoderm to become flatter and narrower in response to the mesodermal signalling (Keller et. al., 1992).

Duprat (1996) modified the classic experiment by Spemann on neural induction to discover a direct correlation between induction by cell dissociation and ectoderm competence. She found that the percentage of aggregates where neurons developed decreased with the age of the dissociated ectoderm. To provide further evidence, reaggregation into 3D structures immediately after ectodermal dissociation led to a 50% reduction of neuronally induced cells. Given only a limited number of neuronal markers were expressed after induction by dissociation, Duprat (1996) concluded that neural induction is not an all-or-nothing event rather a sequence of events that can be experimentally isolated.

Activin is an important mesodermal inducer that forms a morphogenetic gradient to differentiate between the dorsal and lateral endoderm. The ectodermal cells comprise of fibroblast growth factors (FGF) and activin receptors that exhibit competence to activin signalling and mesoderm induction. Activin is important in distinguishing between neural and epidermal fate while follistatin, an activin inhibitor, helps in forming the morphogenetic gradient. As well, L-type Ca^{2+}

channels were demonstrated to be directly involved in the transduction of the neural signal brought on competent animal ectoderm (Duprat, 1996). This pathway involves Ca^{2+} and is controlled by protein kinase C (PKC). Neural tissue formation in axolotl is driven by an increase in internal Ca^{2+} above a threshold value.

1.5 Role of Microfilaments in Cell Shape Changes in Neurulation

Strong evidence suggests lamellipodia to be involved in cell migration during convergent extension where cells intercalate and crawl on top of each other making the entire tissue longer and narrower (Small et al., 2002). This section details the various roles performed by microfilaments in causing cell shape changes and tissue deformation. It then briefly reviews the molecular mechanisms involved in microfilament control and manipulation.

1.5.1 Apical Constriction

Actin monomers polymerize to form microfilaments, a process that is crucial to apical constriction and cellular locomotion. The leading edge of motile cells is dominated by thin actin rich structures called lamellipodia which exhibit highly dynamic behaviour characterized by rapid extension and retraction (Small, 2002). Actin polymerization results in the formation of microfilaments that play a causative role in amphibian neurulation amongst other morphological processes. Cleaving cells as well as apically constricting cells display an ultrastructural distinctive organelle in the form of a ring of microfilaments (Schroeder, 1973). Bottle cells, initially referred as wedged-shaped cells are formed by apical constriction that is fundamental in the process of invagination during gastrulation and neurulation. Schroeder (1973) argues that although invagination is orchestrated by numerous forces, microfilaments alone are sufficient to initiate the processes involved in morphogenetic movements. This proves that microfilaments are important in driving apical construction that is fundamental in neural tube formation.

1.5.2 Different Cell Layers at Various Stages

The different germ layers undergo microfilament-induced shape changes as the embryo develops during neurulation. Neurulation is the process by which the presumptive neural tissue converges and extends to form the neural tube and the neural crest cells. In *Xenopus laevis,* the presumptive neural plate consists of two cell layers, the superficial layer and the deep layer (Schroeder, 1970). The superficial layer is separated into median and intermediate layer; both of which have cuboidal cells prior to neurulation. Cells in the median superficial layer undergo apical constriction thereby changing its shape to narrow and wedged. The cells of the deep layer are seen to be columnar in the dorso-ventral direction and eventually become narrower mediolaterally as development proceeds. The distribution of microfilaments and dimension of cells in the neural plate as development proceeds from stage 13 to stage 18 was elucidated by Karfunkel, (1971) using electron microscopy and discussed below.

Stage 13 *Xenopus* embryos mark the start of the neural plate formation. The cells of the superficial layer have focal junctions within the wide intercellular spaces (Karfunkel, 1971). A circular band of 60Å filaments can be seen in the apical portion of the dorsal cells. These microfilaments are now known to cause apical constriction, to produce a flask-like shape in the advent of neurulation. Bundles of microfilaments are lost in the presumptive epidermal cells (Burnside, 1973). Direct correlation of apical constriction and invagination caused by microfilaments was demonstrated by Burnside (1973), in newt embryos, *Taricha torosa*. Early neural plate explants were cultured in a simple salt solution with their basal side exposed to the medium. Contrary to the normal location of microfilaments in the apex, bundles were observed at the basal ends. The basal constriction curled the whole epithelium towards the basal surface. The microfilament bundles grew thicker as the basalward curling continued until the epithelium folded back upon itself and the basal surface was no longer exposed (Burnside, 1973). At stage 15 *Xenopus*, when the neural groove is formed, the median superficial cells are completely wedged-shaped (Karfunkel, 1973). Even though intercellular gaps are seen, the dorsal junction is still tight. There is a decrease in mitochondrion and yolk granules in the apical cytoplasm. In conjunction with the 60Å filaments, bands of 70Å microfilaments, also known as tonofilaments has been observed (Karfunkel, 1973).

At stage 18, late neural groove *Xenopus* embryo, the median superficial cells are bottle-shaped. They are at least twice as long as wide and intercellular gaps are rare. Mitochondria and yolk granules are entirely absent from the apex. The apical microfilaments are very dense at this time. Intermediate superficial cells have shapes which appear to be distorted as a result of pulling force exerted at the base of the groove. Desmosomes are sometimes seen in these cells, often having keratins and intermediate filaments associated with them (Karfunkel, 1973). At stage 20, when the neural tube is completely closed, all the cells are oriented radially to the lumen of the tube (Karfunkel, 1973). Microfilaments are no longer present in the apex of the cell, however are present in the median superficial and intermediate superficial layers right above the dorsal part of the neuroceol. Concentration of the microfilamentous bands at stage 20 is notably less than they were at stage 13 in the dorsal superficial layer.

1.5.3 Mechanism of Microfilament Alignment

The mechanism that controls microfilament orientation and location has intrigued scientists in the past 30 years (Burnside, 1973; Schroeder, 1973; Karfunkel, 1971). Burnside, (1973) demonstrated that apically constricting cells cause the neural plate to curl inward. However, the mechanical implications of simultaneous apical constriction in the dorsal median layer cells are very complex. Schroeder (1973) suggests a variety of temporal and geometrical factors are involved in microfilament presence, location and alignment that cause cellular as well as tissue-level deformation. Schroeder (1973) found circular bands of 60A microfilaments just inside the lateral cell periphery and immediately beneath the apical surface. As constriction proceeds, there is an increase in the thickness of the microfilament bundles. In axolotls microfilaments are mostly found at the lateral neural groove which helps in forming the trough-like invagination. Likewise the tendency for the cells to constrict travels medially across the neural plate from the lateral ends. This was demonstrated by Lewis (1947) in an experiment that shows that the neural plate closes prematurely when freed from the lateral ends by surgical incisions. He proposed that the apical layer of the neural plate was contractile in nature. To test this hypothesis more critically, cells where the microfilaments were disrupted by vinblastine sulphate lose the tendency to apically constrict (Karfunkel, 1971 & 1974). Further research has questioned the factors that determine the orientation of the microfilaments (Schroeder, 1973). Initially the microfilaments are randomly oriented around the cytoplasm. Right before “wedging”, the microfilaments form a ring in the plane of the constriction. Schroeder (1973) largely attributes mechanical and geometrical factors to tissue and organ structure rather than intrinsic events that direct

the microfilament array. Factors like N-cadherin and E-cadherin differentiate the neural plate from the epidermal plate can also provide inductive signals. Mitochondrion, absence of pigmented granules, and absence of tonofilaments further influence microfilament orientation.

1.5.4 Molecular Control of Actin Assembly

Cell-cell junctions organized by adhesion proteins and underlying actin cytoskeleton play a crucial role in orchestrating the start of neurulation as well as maintain tissue integrity. Recent studies reconfirm the role of filamin and Arp2/3 complexes in F-actin stabilization of microtubule. Filamin association with transmembrane proteins through the F-actin C-terminus serves as a linker between the membrane and the cytoskeleton (Small et al., 2002). However mechanical consequences of such interactions are still to be measured. Prevailing dogma is that cadherins are linked to the actin cytoskeleton through β-catenin and α-catenin. Even though the current study assumes actin polymerization to be the key component in determining cell shape and morphology, other proteins such as Shroom, GTPase Rap1, (Haigo and Hildebrand, 2003) integrins, cadherins and catenins (Drees et al., 2005) play a prominent role in maintaining structural integrity.

In a recent study by Drees et al. (2005), the current dogma regarding cell-cell junctions has been refuted. It was reported that α -catenin does not bind simultaneously to both E-cadherin-β-catenin complex and actin filaments. The cadherin cytoplasmic domain binds with high affinity to β-catenin which in turn binds with weaker affinity to α-catenin. The α-catenin dimerization domain overlaps with the β-catenin binding domain at the N-terminus. The α-catenin monomer and homodimer show preferential binding to β-catenin and actin respectively. Significant recovery after fluorescence loss in photobleaching experiments showed that a fraction of membrane bound α-catenin dissociated from β -catenin and entered the cytoplasm. Arp2/3 mediated actin polymerization is crucial in lamellipodia formation. However, α-catenin homodimer acts like an antagonistic in lamellipodia formation, by suppressing Arp2/3 mediated actin assembly (Drees et. al., 2005). Figure 1.3 shows the mechanism by which α catenin aids in converting F-actin branches to bundles. These results predict that interactions between the cadherin-catenin complex and underlying actin cytoskeleton in cells are very dynamic rather than being static. Increase in F-actin monomer results in preferential binding to β-catenin-E-Cadherin complex causing in increased E-cadherin mediated cell-cell contact.

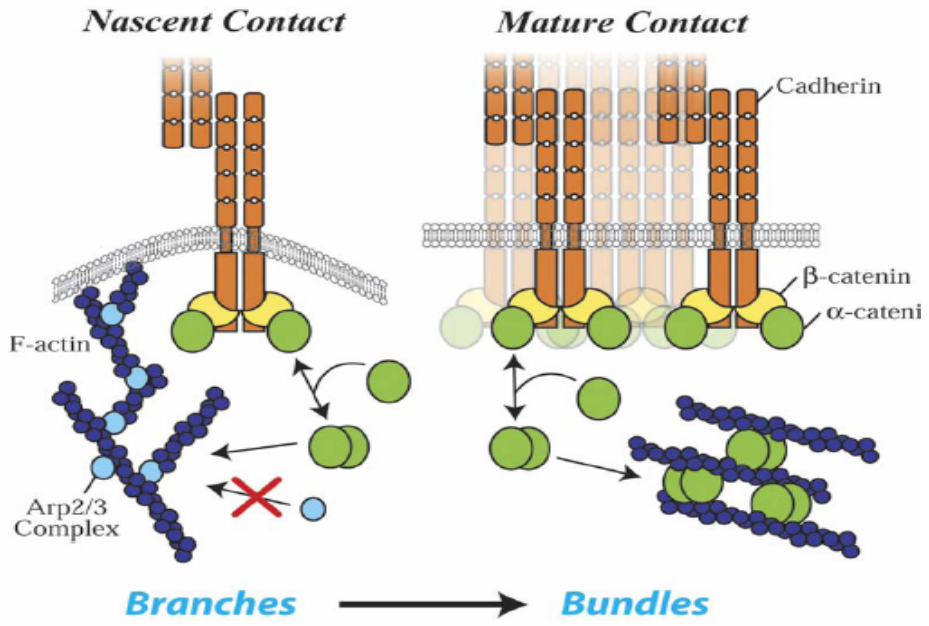

Figure 1.3 Arp2/3 complex regulated actin polymerization. α catenin aids in converting F-actin branches to bundles (Drees et. al., 2005).

The importance of actin polymerization can be supported by the fact that cytoskeletal polymerization and dynamic instability are energetically unfavourable yet conserved. Desai and Mitchison (1997) have reviewed three possible roles for filament function. Basically polymerization allows the cytoskeleton to rapidly reorganize allowing 3-D movement of cells; it provides for a transport mechanism allowing motor proteins to travel along the cell; and lastly it performs mechanical work. Actin polymerization has been shown to produce a force in the cell. According to classical biology, cell movement across each other is a dynamic process where contacts between cells are formed and subsequently broken as they move along each other. These cellular movements are orchestrated by filament polymerization and depolymerization. According to Moore et al. (1995), the force in the tissue causes it to stiffen as it elongates. This theory poses a conundrum regarding the tissue becoming stiff as the integrity of the tissue should diminish as the cells loose contact.

1.6 Effects of Cytochalasin B and Valproic Acid on Microfilaments

1.6.1 Cytochalasin B

Cytochalasins, a group of fungal metabolites, permeate cell membranes and cause cytoskeletal alterations that influence neural development and other defects. Figure 1.4 below shows the structure of cytochalasin B. Intense literature review of the effects of cytochalasin B on tissue morphology and cellular dynamics was done in order to account for the variation in the Young's Modulus in biological aspects due to teratogen treatment.

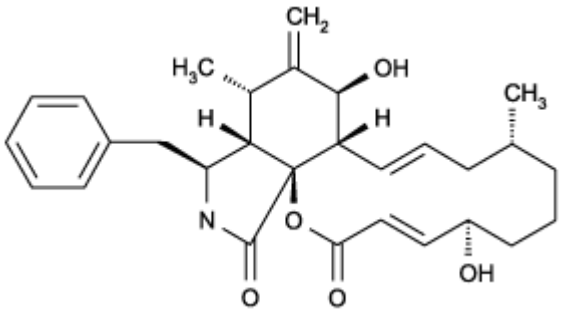

Figure 1.4 Structure of cytochalasin B

1.6.1.1 Biochemistry

Cytochalasins bind to the barbed end of actin filaments, which inhibits both the association and dissociation of actin monomers to that end (Cooper, 1987). The stoichiometry of binding is about one Cytochalasin per actin filament. Electron microscopy of filaments grown from morphologically identifiable seeds has revealed that the major effect of (CB) is at the barbed end as opposed to the pointed end (Cooper, 1987).

Cytochalasin B binds to proteins in a temperature-dependent manner. It associates rapidly with cells and reaches its equilibrium binding level within minutes (Tannenbaum, 1978). It has been reported that the kinetics of binding of radioactive CB to Chinese hamster ovary cells were strongly temperature-dependent; the initial rate was twenty times greater at 37'C than at 0'C. Most of my studies were conducted at room temperature. Despite this pronounced temperature dependence,

binding of Cytochalasin does not appear to require cell metabolism nor is it dependent on active transport.

Further studies of cytochalasin binding to intact mammalian cells demonstrate a non-linear dependence on the concentration of the drug present (Tannenbaum, 1978). The concentration variation can be because there are two binding sites, saturable high-affinity and a low affinity (possibly unsaturable) site on the Chinese hamster ovary cells (Tannenbaum, 1978). Due to these differences it was very difficult to obtain a correlation between our values; however the embryos were treated with two different concentrations of CB. Radioactive CB tests have been performed at a concentration range of 0.005 to 50 ug/mL. For my experiments the concentrations at which the embryos were tested was 2.5 and 5 ug/mL of cytochalasin B dissolved in 10% Steinberg's solution.

The binding of cytochalasin B varies according to the cell/tissue type: The binding of cytochalasin B to HeLa cells, red blood cells and platelets was found to be rapid and reversible at high (10^{-5} M) and low (10^{-7} M) concentrations of the drug. The binding of various types of cells was studied by Lin and Spudich (1974), using drug concentrations ranging from 10^{-9} M to 10^{-4} M. Their results show that mammalian cells express a class of high-affinity binding sites and a class of low-affinity binding sites. In contrast, the binding curves for nonmammalian cells show that they bind cytochalasin B only with low affinity while bacterial cells bind very little of the drug even at high drug concentration. Further analyses to locate the binding of cytochalasin B to cellular components were performed by Lin and Spudich (1974) on bovine platelets. The nucleus revealed negligible cytochalasin B binding activity. Mitochondrion supernatant also bound low levels of the drug. Further studies by Puszkin et al. (1973) have shown strong binding of cytochalasin B to myosin and actomyosin. Interestingly it was observed that actin and cytochalasin B compete for the same site on myosin and that actomyosin complex is resistant to cytochalasin B.

Cytochalasin B was found in the cytoplasm, predominantly attached to the endoplasmic reticulum and cell membrane using radioactive labelling and cell fractionation (Tannenbaum et al., 1973). Resistance of intact membrane proteins to enzymatic degradation upon cytochalasin B binding reveals that these proteins are on the inner surface of the membrane or between the lipid bilayer, but are not exposed to the outside (Tannenbaum et al., 1975; Lin and Spudich, 1974). Another model

suggested that the hydrophobic cytochalasin B might enter and destabilize the lipid bilayer, thus weakening the cleavage furrow (Bluemink, 1971).

1.6.1.2 Disruption of Microfilaments

Cytochalasins can affect the characteristic properties of purified actin and myosin as well as the mutual interaction of these two proteins. Cytochalasin B-bound actin has the following properties in comparison with normal actin filaments: decreased viscosity, low ATPase activity, instability to negative staining, decreased ability to activate myosin ATPase (Spudich and Lin, 1972; Tannenbaum, 1975 and Weihing, 1978). Evidence regarding cytochalasin B interaction with actin has been provided by Weihing (1978) using sucrose density gradient centrifugation of cell extracts. Furthermore cytochalasin does not cause dissociation of actin from plasma membrane of living cells (Tannenbaum, 1975).

The effect of cytochalasin B on lowering the viscosity of actomyosin was demonstrated by Spudich and Lin (1972) in two different experiments, with the help of salts which are commonly used to induce polymerization. In the first, the actomyosin complex was formed before the addition of cytochalasin B while in the second experiment the actomyosin complex was allowed to form after cytochalasin B addition. Addition of actin to myosin in a 5:1 molar ratio caused an increase in the viscosity of the solution to a value of 3.1mL/mg - far greater than the independent value of actin or myosin alone. ATP promoted the dissociation of the atomyosin complex; however, actin and myosin reassociated within 30 minutes. Addition of cytochalasin caused a large and rapid decrease in the viscosity of the actomyosin complex. In the second experiment, the viscosity of myosin alone was not affected by the addition of cytochalasin. Addition of actin to the mixture of myosin and cytochalasin in the presence of 0.5M KCl resulted in the formation of an actomyosin complex that had a viscosity much lower than that obtained in the absence of cytochalasin B. The above experiment demonstrates that cytochalasin B does not interact with myosin and that it does not affect the ATP-assisted dissociation of the actomyosin complex. cytochalasin B binds to the actomyosin complex via actin. The interaction of actin with CB is concentration-dependent as the reduced viscosity of actin in the presence of CB increases with increased actin concentration. This is explained by the increase in actin polymerization caused by competitive inhibition. The final viscosity attained was independent of the initial polymerized or unpolymerized state of the actin filament. However, in contrast, the viscosity of actin remained unchanged in the presence of regulatory proteins troponin and tropomyosin when

treated with cytochalasin. This suggests that regulatory proteins protect actin from the effects of cytochalasin B.

It is interesting to note the effect of cytochalasin B on other cellular structures like myosin and tubulin. In contrasts to its marked effects on actin, cytochalasin B does not affect myosin from striated muscle (Spudich and Lin, 1972). However cytochalasin D does exhibit binding to myosin and inhibiting the activity of ATP sites. Recently it has been found that concentration of cytochalasin B of 1uM or less can inhibit actin-related gelation of cytoplasmic extracts (Weihing, 1976). Most investigators of cytochalasin activity have emphasised interaction with actomyosin sites, however another study demonstrates the binding of cytochalasin A to microtubule. cytochalasin B has not shown such interactions, but incubation of cytochalasin A with 2-mercaptoethanol converts it to CB.

1.6.2 Valproic Acid

Valproic acid, (2-n-propyl pentanoic acid, VA is a widely used antiepileptic-drug that has also been shown to be useful in the treatment of manic depressive illness and migraine (Walmod et al., 1999). Valproic acid is also known to inhibit histone deacetylase, a protein involved in chromatin remodelling. The following diagram shows the chemical structure of valproic acid.

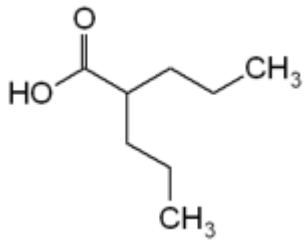

Figure 1.5 Chemical structure of valproic acid

Valproic acid was chosen as a drug for this study, because of its influence on cell motility and cytoskeletal alterations. Walmod et al., (1999) has shown that long-term exposure of fibroblastoid L-cell to VA stimulated actin stress fibre formation, and caused an increase in F-actin concentration. Furthermore, this study revealed that valproic acid caused an increase in focal adhesion formation and

cell-substratum adhesion. Exposure to VA and VA analogues induce an increase in cell area and decrease in cell motility in a manner correlating with the teratogenic potencies of the individual compounds (Berezin et al., 1996). Cells treated with Cytochalasin D roundup due to absence of actin filaments, however VA induced cells pre-treated with Cytochalasin D acquire a star-like shape (Walmod et al., 1999).

Gelsolin is a key protein involved in F-actin dynamics. Investigation of gelsolin in control cells and VA treated cells revealed that VA treatment caused a redistribution of gelsolin in cells (Walmod et al., 1999). In control cells the protein is mainly localized in peripheral membrane ruffles, whereas gelsolin in VA treated cells exhibited a diffuse peri-nuclear localization. Consequently, it can be inferred that the VA induced alteration in the gelsolin regulated dynamics of actin filament contribute to the reduced motile behaviour and altered morphology of VA treated cells. Immunocytochemical stainings of β-tubulin in the presence of VA showed no changes in the concentration or organization of microtubules as a result of the drug treatment (Walmod et al., 1999). This suggests that the changes in the material properties are not due to microtubules but due to microfilament alterations.

1.7 Phalloidin Binding to F-actin Filaments

Phalloidin is a toxin prepared from the *Amanita phalloides* ("Death Cap") which is one of numerous poisonous species of mushrooms in the genus *Amanita* (Molecular Probes, 2007). Phallotoxins are a group of bicyclic hepatapeptides from poisonous mushrooms (Cooper, 1987). Phalloidin binds specifically to microfilament actin (F-actin), inhibiting its depolymerization, and therefore a very convenient tool to investigate the distribution of F-actin since fluorescent analogs can be synthesized that retain actin binding. Fluorescent phallotoxin derivatives such as Alexa Fluor phalloidin conjugates stain F-actin selectively at nanomolar concentrations and are readily water-soluble, thus providing convenient probes for identifying and quantifying actin in tissue sections, cell cultures or cell-free preparations. The Alexa Fluor phalloidin conjugates are superior in brightness and photostability to all other spectrally similar conjugates tested (Molecular Probes, 2007). Moreover, Phalloidin has further advantages over antibodies for actin labeling, in that its binding properties do not change appreciably with actin from different species, including plants and animals; as well as, its non-specific staining is negligible; thus, the contrast between stained and unstained

areas is high. Furthermore, it does not bind to monomeric G-actin, unlike some antibodies against actin (Adams and Pringle, 1991).

Phalloidins do not permeate cell membranes and have not been very useful in living cells (Cooper, 1987). Cells treated with phalloidin show a variety of toxic effects and often die. Furthermore, phalloidins affect the dynamics of actin polymerization and stability. The primary target of phalloidin is actin filaments. This makes phalloidin an excellent marker to visualize actin polymerization. Phalloidin binds to actin filaments much more strongly than actin monomers shifting the equilibrium towards filaments as opposed to monomers. It lowers the critical concentration for polymerization by 10- to 30- fold under various conditions (Cooper, 1987). Phalloidin causes a decrease in the dissociation rate constant at both the barbed and pointed end, however contrary to a decrease in the critical concentration phalloidin causes a decrease in the association rate at the barbed end by 20% (Cooper, 1987).

The stoichiometry of binding is one phalloidin for either one or two actin protomers. Phalloidin protects actin filament from depolymerization. Since our samples were treated with phalloidin after the embryos were already fixed, phalloidin was unable to alter the concentration or the filament state of the actin molecules. It is challenging to infer the exact association and dissociation rate constant, as well as the stoichiometry of binding, since the value varies according to the method employed and the purity of the sample. Furthermore, photoactivatable derivatives of phalloidin, bound to actin filament, react covalently with amino acids Glu-117, Met-119, and Met-355 (Cooper, 1987).

1.8 Neural Tube Defects and Real Life Implications

The process by which the neural tube closes is species-specific. In amphibians there is one site where the neural tube starts to close leaving two neuropores as the tube zips up in both directions. In birds there are about three different sites of closure: anterior neuropore, posterior neuropore and the auditory placodes. In mammals, there are several points of closure of the neural tube, which provide backup mechanisms in case one closure site fails. Diet, environmental factors as well as genetics play crucial roles in the closing of the neural tube. According to Schoenwolf (1994), closure is not a

smooth process. This sections looks at common neural tube defects and real life implications to clinical research.

1.8.1 Genes that Cause Neural Tube Defects

Neural tube defects can be seen in a variety of different forms. In order to understand these defects, it is crucial to identify and characterize animal models that are reflective to the diversity of defects seen in humans.

As discussed in the previous chapter; the expression pattern of cell adhesion molecules; N-cadherins and E-cadherins mark the separation of the ectoderm into neural and epidermal tissue. Cell adhesion molecules follow the rule of differential adhesion molecules between the neuroepithelial cells of the neural tube and the surrounding non-neural ectoderm allowing for cell sorting and separation (Papalopulu and Kintner, 1994). Over-expression of N-CAM and N-cadherin in *Xenopus* ectoderm exhibited a dominant negative effect on morphology. RNA expression in ectodermal cells showed the presence of cell boundaries that were largely absent in subpopulations of ectodermal cells (Detrick *et. al.,* 1990). This shows that cadherin misexpression can cause neural tube defects.

X-dll3, X-bar and F-actin are localized in the neural plate and could possibly be involved in neural tube defects. Whole-mount *in situ* hybridization of *Xenopus* neurulating embryos demonstrates the presence of homeobox transcript *X-dll3* in the anterior ridge of the neural plate (Papalopulu and Kintner, 1994). The portion of the anterior neural plate expressing *X-dll3* has been shown by cell fate mapping to give rise to anterior neural tube and the olfactory placodes. Similar results have been obtained using *X-bar*, another *Xenopus* homeobox gene product. *X-bar* expression has been localized in the anterior neural plate and the dorsal section of the developing eye (Papalopulu and Kintner, 1994). One model suggests that transcription factors as well as membrane proteins form a morphogenetic gradient that regulate downstream gene targets and cause cell differentiation. A novel cadherin called F-cadherin has been seen in the nervous system. F-cadherin is localized in the cell boundaries that subdivide the neuroepithelium into different regions and is detected in the neural plate stage (Papalopulu and Kintner, 1994).

1.8.2 Embryonic Mechanisms of Neural Tube Defects

Anomalies in neural tube development can give rise to many diseases such as spina bifida and anencephaly. Apart from determining aetiological factors responsible for neural tube defects, errors during embryonic development contribute significantly towards NTD. The best-understood category of neural tube defects, in terms of the underlying embryonic basis, comprises spina bifida and associated caudal defects (Copp, 1994). Spina bifida is a serious congenital anomaly frequently associated with significant neural defects. A critical event in neural tube development in the lower spinal region is the transition between primary and secondary neurulation. The transition between the two models of neurulation occurs at the site of posterior neuropore closure in the upper sacral region of the mouse (Copp & Brook 1989). Furthermore the most consistent neural tube defects appear to derive from failure of the neural tube to close dorsally or the reopening of the neural tube in the caudal-section.

Chapter 2: Methods

2.1 Staging Phenotypic Variations

Axolotl embryos were imported from the Ambystoma Genetic Stock Center, University of Kentucky, where they were bred specifically for research. All research was carried out in accordance with the University of Waterloo Animal Care Committee and the Canadian Council on Animal Care. On arrival, embryos were placed in 20% Holtfreters Solution and stored at 4˚C. Both tests, drug treatment and tissue stretching, were conducted at room temperature. Axolotls were staged to ensure that all the embryos were at the same developmental stage according to Bordzilovskaya *et al.* (1989). Embryos from each test were kept under identical temperature conditions to produce similar development, while the rest were stored in the fridge. This allowed successive tests to be carried out from the same batch of embryos. Formation of the neural cleft marked the onset of neurulation and was labelled as stage 13 embryos. Embryos exhibiting the neural cleft were selected for the experiment.

2.2 Drug Treatment

In order to alter the F-actin filaments, embryos were treated with one of two different concentrations of cytochalasin B (2.5ug/mL and 5ug/mL) or one concentration of valproic acid (5mM). Morphological changes due to teratogen treatment on axolotl neural development are the first indication of abnormal growth. Embryos exhibiting neural tube defects were photographed and then selected for further testing. Embryos that failed to demonstrate a phenotypic defect were discarded.

Phenotypic analysis of cytochalasin B treated embryos involved cystein treating (2% solution at pH8) or mechanically removing the jelly coat. The vitelline membrane was allowed to remain during this stage. The embryos were then placed in 2.5 and 5ug/mL concentration solutions of cytochalasin B (VWR) dissolved in DMSO and diluted in 20% Holtfreters solution. The control embryos were treated with 10% Steinberg's solution (10mL of DMSO in 90mL of 20% Holtfreters solution). The embryos were treated at stage 13, maintained in the solution for one hour at room

temperature after which they were washed with 20% Holtfreters solution then allowed to develop to stage 15. Once the controls reached stage 15, some embryos were fixed in 4% paraformaldehyde for further phenotypic analysis. The remaining embryos were then used in the tissue stretching device. Embryos treated with cytochalasin B were only tested for neural tube defects from stage 15 to tail bud stage.

Stage 13 axolotl embryos were also treated with 5mM valproic acid (VWR) dissolved in 10% Steinberg's solution. Similar to cytochalasin B, the drug-induced embryos were washed after 1 hour of incubation. They were then allowed to develop until the controls reached stage 15. At this point, some of the embryos were fixed with 4% formaldehyde while the rest were used in the tissue stretcher.

2.3 Measuring Tissue Properties

This study uses a novel instrument (Wiebe, 2003) to measure the mechanical properties of axolotl-tissue samples. The instrument can measure the tensile properties of tissue samples as small as 300 to 500 um in length. Tissue testing was performed to correlate the mechanical changes in the cytoskeletal structure of normal versus teratogen treated tissues. The first step of the experiment included straightening the wire to remove kinks and curvature. The wires were then glued on the acrylic arms attached to the motorized Zaber (a control system that can move in one direction). Once the instrument was ready, the devitellinized embryos were placed directly beneath the wires, on a pedestal, in the Petri dish filled with 20% Holtfreters solution. With the help of another device called the wire-lifter, the wires were lifted out of the solution to apply glue on them. The glue-coated wires were then gently placed on the embryos before stretching. Once the embryos were glued in position, the Zaber was turned on and pictures were captured every 30 seconds while the tissue was being stretched. The entire movement was controlled by Tissue GUI; a software made by our laboratory. This instrument has made possible the first measurements of the mechanical properties of embryonic epithelium and allows investigation of uni-axial stress strain characteristics and their dependence on cytoskeletal structures.

The instrument uses a pair of cantilevered wires to which the specimen is glued. In order to measure the stress in the tissue, one of the wires is moved under computer control using a motorized stage. Figure 2.1 and Figure 2.2 show the positioning of the Zaber, lab jack, cantilever wires, Petri dish and acrylic arms in the tissue stretching device. Force in the specimen is calculated from the lateral displacement in one of the wires. The gluing process uses a custom device that lifts the wires out of the medium so that cyanoacrylate glue can be applied to the end of the wires before they are snapped back to their original position where they can be attached to the embryo. The entire set up was positioned using a robotic camera system. The system was devised so that high magnification images could be obtained to produce ultra high resolution over the entire specimen.

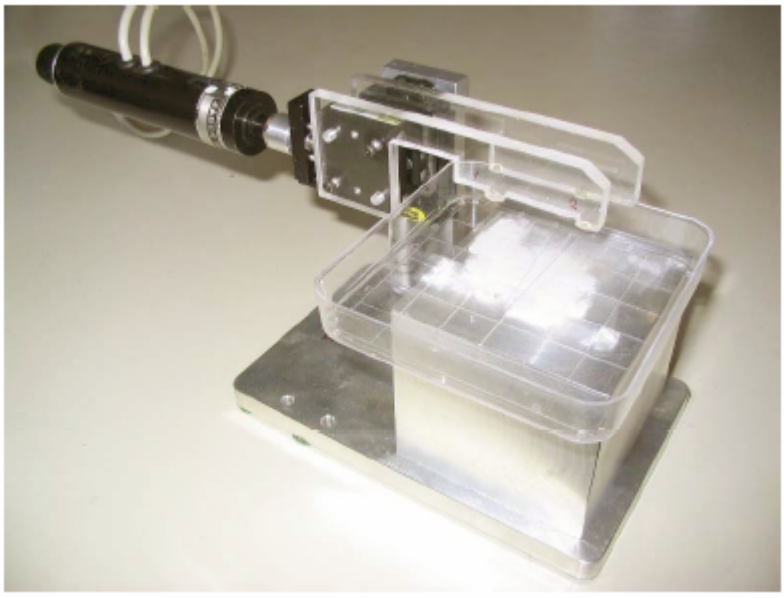

Figure 2.1 Side view of the tissue stretching device. Picture taken from Wiebe, (2003)

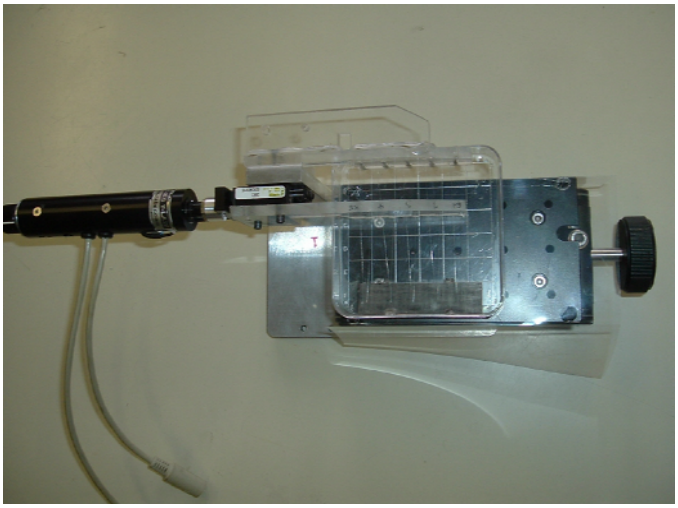

Figure 2.2 Top view of the tissue stretching device. Picture taken from Wiebe, (2003)

2.3.1 Straightening the Wire

The wire was first straightened using a pair of fine forceps that aids in tweaking the kinks out and straightening the naturally occurring curvature. For the test reported, stainless steel wires having diameters of 100 or 125 um were used with lengths between the ranges of 60 - 74mm. The force was calculated by treating the more flexible wire (100um) as the deflecting cantilever beam with a point load (F) at its end having an end deflection d given by

$$F = \frac{3dEI}{L^3} \qquad (1)$$

where E, I and L are respectively the Young's modulus of the wire material, the moment of inertia and the wire length. The thicker and stiffer wire was moved using a motorized system shown below.

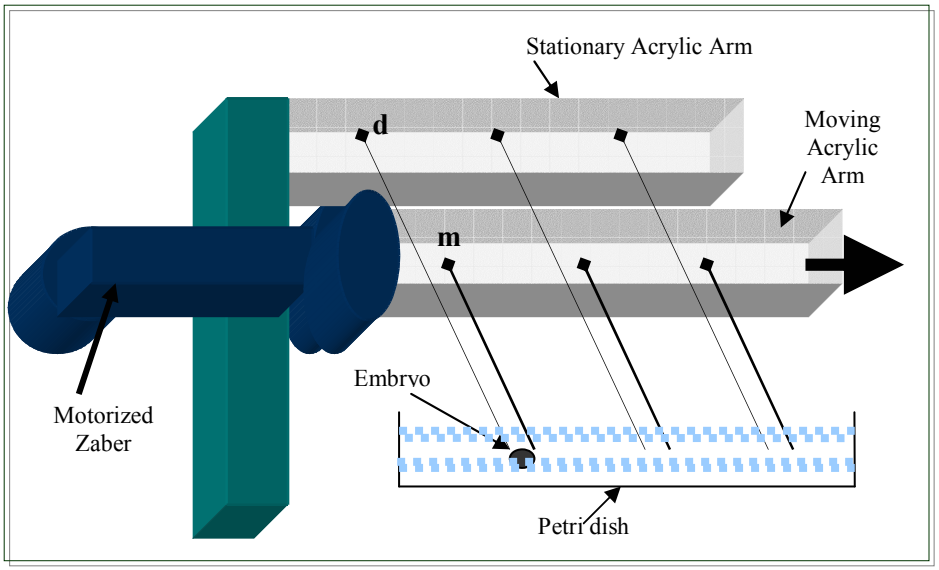

Figure 2.3 Shows the wire setup. d is the long flexible deflecting wire (100um) and m is the thick moving wire (150mm).

2.3.2 Attaching Wires to Zaber/Stretching Device

Attaching the wires to the Zaber is an intricate process requiring extreme manual dexterity. Before attaching the wires to the acrylic arms, the Zaber was retracted to the home position, leaving a little room for allowance. Once the acrylic arm was positioned such that the thin stationary wire was before the thick moving wire, the Zaber with the metallic pedestal was removed from the base. The Zaber and arm were allowed to rest upside down on round weights, with smaller weights used to place them in the appropriate position (Figure 2.4). The wire plate is an acrylic base that has the correct wire orientation engraved on it. The acrylic plate was glued on the lab jack, and brought up to the desired height. The thick wires were first placed on the left side of the plate. Using a swift movement, sticky tape was applied to fix the position of the thick wires. At this point, extra wire length was cut off with a wire cutter. The thick wires were then glued on the acrylic arm using a hot glue gun. The tape was slowly removed. The longer thinner wires were placed on the right hand side of the plate. The longer wires were clamped between the acrylic arm and a flat plate. Once correctly oriented, the thin wire was screwed down. Extra thin wire was trimmed at this step. The Zaber was then fastened to the stationary aluminium base. A sheet of transparency was used to cover the lab jack to protect it from water. A square Petri dish was placed between the transparency and cantilever wires on the lab jack. The Petri dish consists of a small movable base that allows the embryo to rest on it. Finally the Petri dish was filled with 20% Holtfreters solution.

Figure 2.4 Gluing the cantilever wires on the acrylic arms prior to assembly. Picture taken from Wiebe (2003).

2.3.3 Gluing Embryo to Wire

A wire lifter was another novel device that was used to glue the wires on the embryo in the Petri dish. Before the wires were glued, it was important to ensure that the Zaber was at its home position leaving a little room for initial jerks. Stage 15 embryos were stretched in the anterior-posterior and medio-lateral directions at a rate of 50% per hour. Figure 2.5 shows the side view of the experimental setup. Once the wires were glued, and the embryo was in place, the wire-lifter was gently removed from the medium. At this point, the extra tissue including the underlying mesoderm cells were excised. As the tissue was left freely suspended in the solution, the lighting was adjusted and the camera focused.

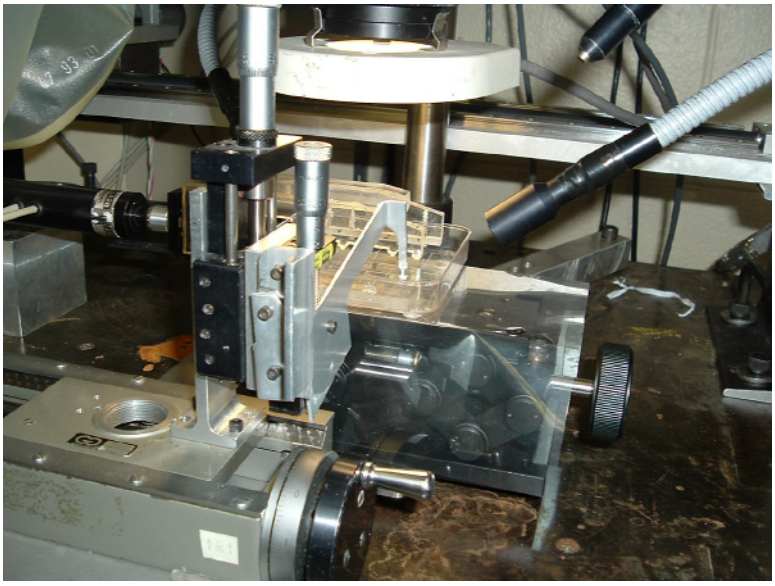

Figure 2.5 The side view of the experimental setup before operation. Image attained from Wiebe (2003).

2.3.4 Tissue GUI

Once the setup is complete, the Tissue GUI software is then started. The Tissue GUI program controls all the motorized stages and actuators, capturing the images of the embryo being tested and processed in real time, outputting images of tissues and wire position data over time. The Tissue GUI software was written by Jim Veldhuis and Colin Wiebe.

2.4 Phalloidin Staining

In order to visualize the cytoskeletal structure in the ectodermal layers, cells were stained with phalloidin which binds to polymerized F-actin filaments. Embryos were fixed in 4% paraformaldehyde (PA), fractured along the dorso-ventral margin, washed with 1x PBS and then fixed again in 4% PA, washed in PBS and then permeablized in 1% Triton X. 4% BSA was used to block non-specific binding that contributes to high background staining. The embryos were then incubated for 3 hours in Alexa fluor 488 phalloidin (Molecular Probes). Later the embryos were observed under a confocal microscope.

2.4.1 Preparation of 10x Phosphate Buffered Saline (PBS)

10x Phosphate Buffered Saline (PBS) Stock Buffer was prepared using the following salts:

Table 1 Contents of PBS stock buffer

Salt	Amount (grams)	Final [mM]
NaCl	80	1368.7
Na_2HPO_4	14.4	101.4
KCl	2.0	26.8
KH_2PO_4	2.4	17.6

The above salts were dissolved in ~800 ml deionised distilled water (ddH_2O) by stirring. The pH was adjusted to 7.4, using conc. HCL or conc. NaCl, and the final volume was brought to 1.0 L and stored at room temperature. PBS was diluted to 1x and used for making solutions and washing tissues.

2.4.2 Preparation of Axolotl Embryonic Tissue for Fixation and Labelling

Before staining the embryo the vitelline membrane was removed. Fine Sharpe forceps were pierced into the transparent gel surrounding the vitelline membrane (VM) while holding the embryo in position. Then, using another pair of forceps, the jelly coat was stretched apart to remove the embryo from the gel. The dejellied embryo was transferred to a disposable scintillation vial (20 ml) (Kimble Glass INC.) containing fresh 1x PBS buffer. The embryo was rinsed once with 1x PBS and the VM removed under a dissecting microscope using a fine Sharpe forceps. Removal of the VM can be performed after the first fixation of the whole embryo in 4% paraformaldehyde (PA)

2.4.3 Fixation and Permeabilization of Axolotl Embryos

After dejellying, the embryos were fixed and washed. The whole embryo was fixed in freshly made 4% PA for 1-1.5 h. The PA was dissolved in 1x PBS pre-heated to ~ 70-80^{o}C by stirring on a stirring plate set at “low” heat. The pH was then adjusted to 7.2 and used for tissue fixation. During detergent treatment or washing, the embryos were gently agitated intermittently or on slow 3-dimensional

motion of a nutator. The embryos were washed in 1x PBS three times for 5 minutes each. After which the embryos were transferred into a 35 cm^2 Falcon Petri dish (Becton Dickinson Co.)

Staining was performed on whole embryos since we were concerned with the outer ectodermal layers. Using a blunt forceps the embryo was then transferred to the vial containing 1x PBS (1/3 of the volume). The embryo gently rinsed twice with 1x PBS. The tissue is washed again three times for five minutes each. The embryos is permeabilized in 1% TritonX-100 in 1x PBS for 20 min. Finally the tissue is washed in PBS three times for five minutes each.

2.4.4 Labelling of F-Actin with Alexa Fluor 488 Phalloidin Probe

The next step involves labelling the F-actin with Alexa Fluor 488 (Molecular Probes). The embryo is first blocked in 4% BSA in 1x PBS (after filtered using No. 1 filter paper) for 2 h. This minimizes non-specific binding that contributes to high background staining. The embryo is incubated for 1-1.5 h in Alexa fluor 488 phalloidin (stock diluted at 1:50) in 1x PBS- 4% BSA) at R.T. The stock, 300 U Alexa fluor 488 phalloidin, was dissolved in 1.5 ml 100% Methanol chilled at –20^{o}C. The stock as well as a recovered working solution of Alexa fluor 488 was stored at $\leq$ -20^{o}C. Also, from this step onwards, all procedures were carried out in the dark since the fluorochrome is light sensitive. The embryo was then washed three times (5 minute each) and transferred to a Petri dish.

2.4.5 Evaluation of F-Actin Signal and Analysis of its Distribution

The F-actin signal was then visualized using a Zeiss LSM 510 META confocal microscope. Alexa fluor 488nm at 13.9% was viewed at the narrow range of 505-530nm as well as the wide <530 nm. The Pin Hole Ch2 was set to 47um and the filter was set to LP505. The images were viewed under a 10x C-apochromat objective (NA = 0.45). The same setting was used to visualize all the images in order to achieve the most accurate comparison of the control embryos with the teratogen treated embryos. The images were then cropped-scanned to a maximum zoom of 3.0. The images were viewed with the help of Zeiss LSM Image Browser version 3.6 downloaded from the following website: http://www.embl-heidelberg.de/eamnet/html/body_image_browser.html

2.5 Calculations

The stiffness of the tissue was characterized by its Young's Modulus. The Young's Modulus describes the tensile elasticity or the tendency of an object to deform along an axis when opposing forces are applied along that axis. The tangential Young's Modulus is defined as the ratio of incremental true stress to incremental true strain. Stress is defined as an applied force or system of forces that tends to strain or deform a body. Strain is a deformation produced by the stress induced. To obtain the true stress and true strain values, it was first necessary to generate force-displacement curves (Figure not shown). Forces were determined using Eqn (1) and displacements from Eqn (4). From the force-displacement calculations, values of stress and strain were derived. Engineering stress and strain measurements incorporates fixed reference quantities. These values apply to tissues that do not deform. True stress and strain measurements account for changes in the cross-sectional area caused by tissue deformation, giving more accurate measurements for events such as tensile strengths. Engineering stress and strain uses the initial area while true stress and strain uses the final area as the tissue stretches.

2.5.1 Force

The force was calculated using the beam deflection in the wires as they pulled the tissue apart using the formula below. Where d is the wire deflection, E is the Young's Modulus, I is the Moment of Inertia, L is the length of the tissue and F is the force.

$$F = \frac{3dEI}{L^3} \quad (1)$$

Engineering Stress Resultant

The force values were then used to determine the engineering stress resultant using the following equation. Where σ_{Eng} is the engineering stress resultant, F is the force and W is the width of the sample.

$$\sigma_{Eng} = \frac{F}{W} \quad (2)$$

The engineering stress resultant σ_{Eng} is a measure of force over specimen width as opposed to area. Since the thickness of the tissue varied greatly it was hard to measure. In order to minimize approximations, this measurement was entirely removed from our calculation and the Engineering Stress Resultant was used σ_{Eng}. The true stress resultant, σ_{True} was then calculated using the following formula, where ε_{Eng} is the engineering strain.

$$\sigma_{True} = \sigma_{Eng} (1+ \varepsilon_{Eng}) \quad (3)$$

2.5.2 Tissue Deformation

The next important measurement was tissue deformation D_{Tissue}. In order to determine the tissue deformation, three different methods were tried and the third method was determined to be the most accurate.

Method1: The stress was calculated using the beam deflection formula above. The tissue deformation was calculated using the initial, L_0 and current L_f wire position.

$$D_{Tissue} = L_f - L_0 \quad (4)$$

The value obtained by method one was not in agreement with Wiebe and Brodland (2004). There are at least two important reasons for the discrepancy. Firstly this method assumes the strain is uniform over the entire width of the glued tissue. Since the tissue was not of uniform thickness or width, this is not a particularly good assumption. Second this method assumes that the wire deformation, D_{Wire}, is equal to tissue deformation, D_{Tissue}. This is not always the case due to imperfect gluing. Due to these issues a more rigorous method was needed.

Method2: The stress values were calculated as before, however the tissue deformation value was calculated by tracking a pair of points on the tissue. The tissue deformation, D_{Tissue} was given by the change in the distance between the points as the tissue stretched. This was calculated using the following formula, where L is the distance between the points at time 2.

$$\Delta L_{at\ t=2} = (L_{1.t=2} - L_{0.t=2}) - (L_{1.t=0} - L_{0.t=0}) \quad (5)$$

This method addressed the discrepancy between the wire deformation and tissue deformation, but did not address the issue of non-uniform strains caused by non-uniform specimen geometry.

Method3: Method 3 is similar to method 2 difference being, instead of tracking one pair of points the tissue deformation was measured by tracking five pairs of points distributed across the entire width of the specimen. This allowed for calculation of the average deformation which is more accurate than using earlier methods.

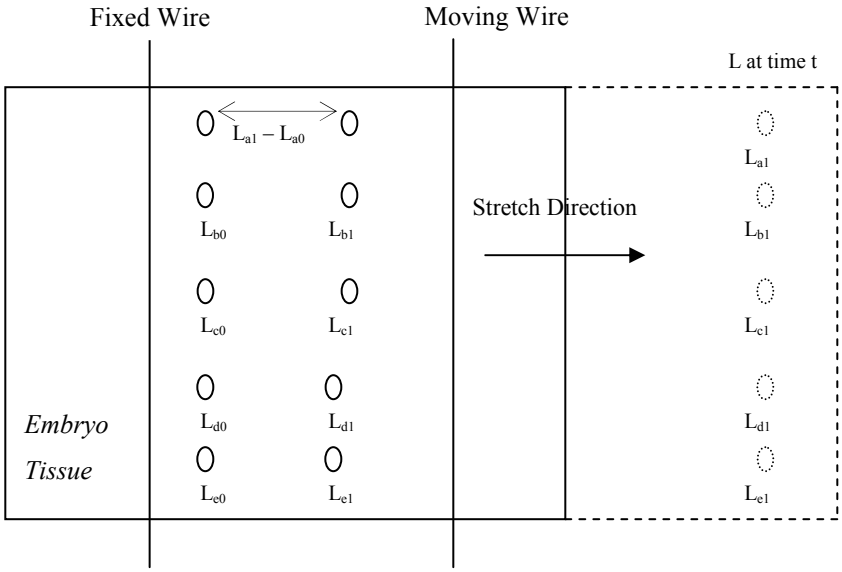

Figure 2.6: Method3; Five pair of points that are tracked over time to measure the engineering strain

$$\Delta L_{at\ t=2} = \text{Average of the value below} \quad (6)$$

$$(L_{a1.t=2} - L_{a0.t=2}) - (L_{a1.t=0} - L_{a0.t=0})$$

$$(L_{b1.t=2} - L_{b0.t=2}) - (L_{b1.t=0} - L_{b0.t=0})$$

$$(L_{c1.t=2} - L_{c0.t=2}) - (L_{c1.t=0} - L_{c0.t=0})$$

$$(L_{d1.t=2} - L_{d0.t=2}) - (L_{d1.t=0} - L_{d0.t=0})$$

$$(L_{e1.t=2} - L_{e0.t=2}) - (L_{e1.t=0} - L_{e0.t=0})$$

Engineering Strain

The tissue deformation values were then used to measure the engineering strain ε_{Eng} using the following formula.

$$\varepsilon_{Eng} = \frac{L_f - L_0}{L_0} \quad (7)$$

The true strain ε_{True} was then calculated using the following equation.

$$\varepsilon_{True} = \ln(1 + \varepsilon_{Eng}) \quad (8)$$

Chapter 3: Results

3.1 Tissue Stretching in Anterior-Posterior and Mid-Lateral Direction

Embryonic neural plates as well as lateral epidermal tissue were stretched in both the anterior-posterior and mediolateral directions. The wires were glued on to the embryo after vitelline membrane removal and then the rest of the fragment was excised using an eye-lash tool. Figure 3.1A & B shows the neural mid-section stretched in the lateral and anterior-posterior direction respectively. The neural cleft can be visualized clearly in all eight pictures. In order to prevent errors caused by inducing forces from the surrounding tissue, the neural cleft and the non-neural ectoderm were completely removed.

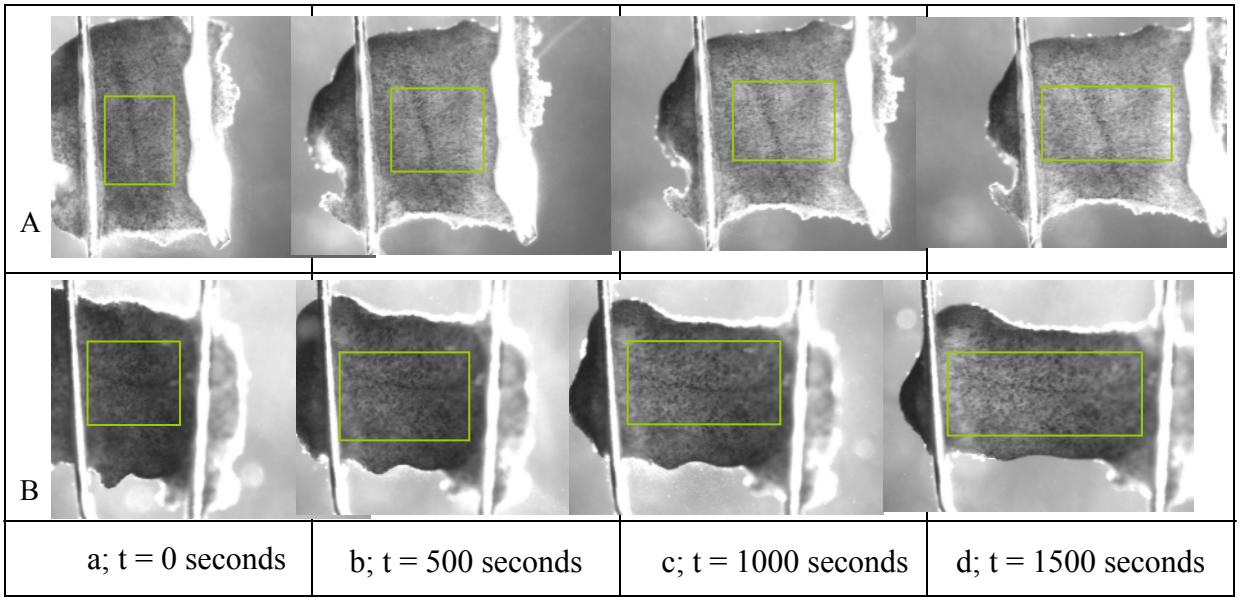

Figure 3.1 Dorsal-Mid section of stage 15 control embryos. A. The embryo being stretched in the lateral direction at various time intervals. B. Another embryo being stretched in the anterior posterior direction. Columns a, b, c & d reveals the embryos being stretched at time 0 seconds, 500 seconds, 1000 seconds & 1500 seconds respectively.

3.2 Sample Calculation

A sample calculation from the dorsal-mid region specimen taken from a Stage 15 control embryo stretched medio-laterally is detailed below.

3.2.1 Calculations to Measure Stress

The forces in the wires were calculated by tracking the deflection of the beam tip over time, where X1 and Y1 are positions of the stiffer-moving wire tips and X2 and Y2 are positions of the deflecting-flexible wire tips at times 1 and 2 respectively.

Table 2 Position of one pair of tracking points over time (seconds).

Time (s)	Awire X1 (μm)	Awire Y1 (μm)	Fwire X2 (μm)	FwireY2 (μm)
2	510	380	169	571
32	513.5	381.25	173.25	571.5

The wire displacement in um is calculated using the following formula.

$$d\ (m) = \frac{10^6(\mu m/m) * \text{Wire Displacement (pixels)}}{\text{Image Scale (pixels/mm)}}$$

$$= \frac{10^6 * (X2_t - X2_0)}{\text{Image Scale}}$$

$$= \frac{10^6 * (173 - 169)}{4.4*10^5\ (mm/m)}$$

$$= 9.09*10^{-3}\ m$$

The force in the deflection beam (F), where d is the deflection, E is the Young's Modulus, I is the moment of inertia and L is the length of the wire:

$$F = \frac{3dEI}{L^3} \quad (1)$$

$$= \frac{3 * 9.09*10^{-3}\ (m) * 1.93*10^{11}\ (Pa) * 5.23*10^{-18}\ (m^4)}{(64(mm)/1000(mm/m))^3}$$

$$= 0.111589*10^{-3}\ N$$

The engineering stress (σ_{Eng}), where F is the force and W is the width of the specimen:

$$\sigma_{Eng} = \frac{F}{(W * 1000)} \quad (2)$$

$$= \frac{0.111589*10^{-3}\ (N)}{(2*10^{-3}(m)*1000)}$$

$$= 5.5794*10^{-5}\ N/m$$

The true stress (σ_{True}), where (σ_{Eng}) is the engineering stress and (ε_{Eng}) is the engineering strain:

$$\sigma_{True} = \sigma_{Eng}\ (1+ \varepsilon_{Eng}) \quad (3)$$

$$= 5.5794*10^{-5}\ (1 + (0.99\%))$$

$$= 5.52*10^{-5}\ N/m$$

3.2.2 Calculations to Measure Strain

Tissue deformation, ΔL, was calculated by tracking 5 pairs of points selected along the entire length of the tissue. Table 3 below shows the position of the ten points over time taken from a stage 15 embryo treated with 5mM valproic acid. The pairs are as follows; X1-X6, X2-X7, X3-X8, X4-X9, X5-X10.

Table 3 Position of the ten tracked points from time t=0 to time t=30 seconds

Time	X1	X2	X3	X4	X5	X6	X7	X8	X9	X10
0	223	233	257	260	262	348	358	392	395	369
30	227	237	261	264	266	351	361	395	398	371

The engineering strain was measured over the first 10% strain relative to the first image. This was done because the Young's Modulus can be obtained from the initial slope of the stress strain graph.

Tissue deformation $\Delta L_{at\ t=2}$ between point X6 and X1 is calculated accordingly

$$= \frac{(X6_f - X1_f) - (X6_0 - X1_0)}{(X6_0 - X6_0)} \quad (7)$$

$$= \frac{(351 - 227) - (348 - 223)}{(348 - 223)}$$

$$= 0.80\%$$

Tissue deformation Δ Lat t=2 between points X7 and X2, X8 and X3, X9 and X4, X10 and X5 is calculated accordingly:

$\Delta L_{at\ t=2}$ between X7 and X2 = 0.90%

$\Delta L_{at\ t=2}$ between X8 and X3 = 0.74%

$\Delta L_{at\ t=2}$ between X9 and X4 = 0.74%

$\Delta L_{at\ t=2}$ between X10 and X5 = 1.75%

The average tissue deformation between all five pairs of points:

$$\text{Avg } \Delta L_{at\ t=2} \quad (6)$$

$$= (0.80\% + 0.90\% + 0.74\% + 0.74\% + 1.75\%) / 5$$

$$= 0.99\%$$

The true strain (ε_{True}), where (Avg $\Delta L_{at\ t=2}$) is the average deformation between all the points at time t = 2 seconds:

$$\varepsilon_{True} = \ln (1+ \text{Avg } \Delta L_{at\ t=2}) \quad (8)$$
$$= \ln (1 + 0.99\%)$$
$$= 0.000110$$

Appendix A contains the values of true stress and true strain obtained during the first 1500 seconds.

3.2.3 Resultant Young's Modulus

The true stress is then plotted against the true strain. The graph is then fixed by a linear fit. The slope of the curve reveals the value of the Resultant Young's Modulus.

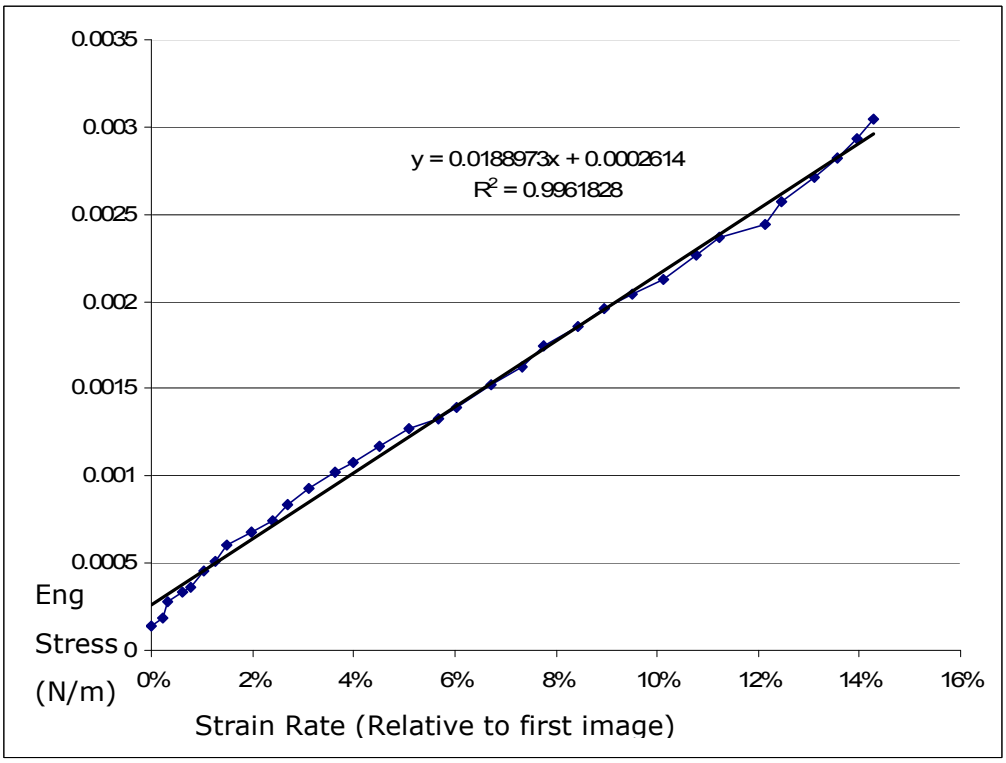

Figure 3.2 Graph of the true stress versus true strain. The slope gives the Resultant Young's Modulus. The above graph is plotted for the first 1500 seconds obtained from the table below.

The Resultant Young's Modulus according to the above graph is 1.8 N/m. The complete values obtained from all the tests have been provided in a table form in Appendix B and graph form in Appendix C. Appendix D shows the wire-lengths and pixel images used for all the tests. Figure 3.3 shows a typical graph of stress versus strain from the beginning of the test until the tissue starts to tear.

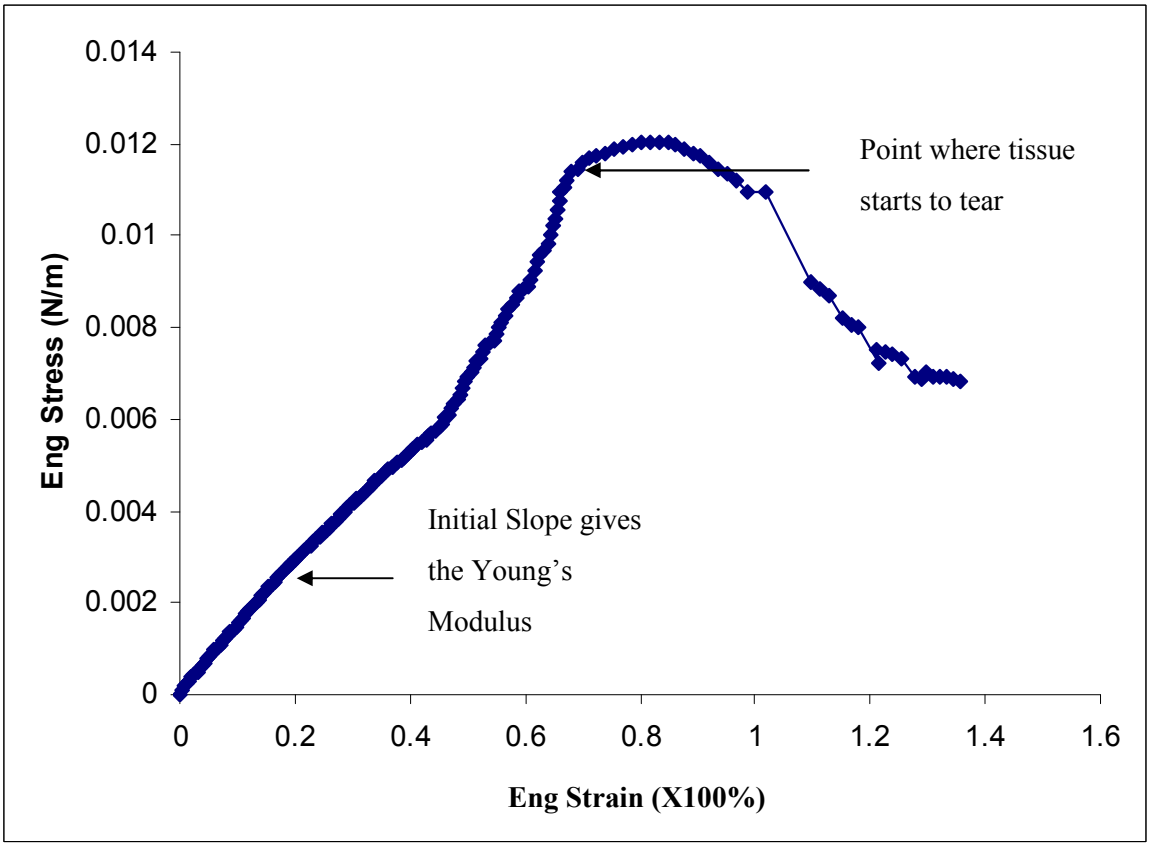

Figure 3.3 Shows the typical stress (N/m) versus strain (X100%) graph of the tissue for the entire duration of the experiment. The initial slope gives the Young's modulus. A sharp decline in the stress is observed at the point where the tissue starts to tear.

3.3 Teratogen Study

3.3.1 Effect of Cytochalasin B on Mechanical Properties

Specimens from stage 15 axolotl embryos exposed to one of the two concentrations of Cytochalasin B were stretched in the medio-lateral or anterio-posterior direction Figure 3.4. The dorsal-mid and lateral-mid regions of the axolotl embryo were investigated. Table 4 and Table 5 summarize the Resultant Young's Modulus of control-embryo tissue compared to teratogen treated mid-dorsal and mid-lateral tissue. Figure 3.5 depicts an increase in the tissue stiffness of the cytochalasin B treated embryos, with an increase of 297% in the mid-dorsal tissue stretched in the medio-lateral direction. Figure 3.6 shows an increase in tissue stiffness when the embryo is treated with 2.5ug/mL cytochalasin B and stretched in AP direction. However embryos stretched in medio-lateral direction, in the mid-lateral tissue, causes the Resultant Young's Modulus to decline in the 2.5ug/mL tissue and increase in the 5ug/mL tissue sample. Data from all 51 specimens are shown in Appendix B, C and D.

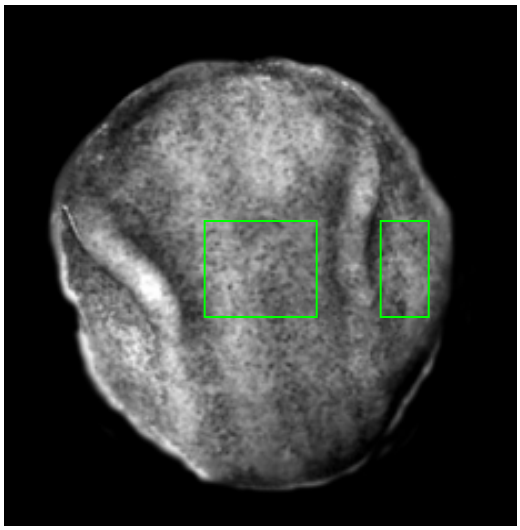

Figure 3.4 Shows the tissue that was stretched. Green box in the center is the mid-dorsal, while the green rectangle on the left is the mid-lateral tissue. Top of the image is the anterior end while the bottom is the posterior end of the specimen.

Table 4 Correlation between cytochalasin B concentration and tensile properties of mid-dorsal tissue

Stretch Direction	Anterior-Posterior			Medio-Lateral		
Drug Concentration	Control n = 4	2.5ug/mL n = 3	5ug/mL n = 3	Control n = 4	2.5ug/mL n = 3	5ug/mL n = 3
Resultant Young's Modulus	5.53	7.98	11.1	4.6	7.32	18.3
Standard Deviation	+/-5	+/-2	+/-6	+/-1	+/-3	+/-7
Percentage Change	--	+43.4%	+100.7%	--	+59.13%	+297.8%

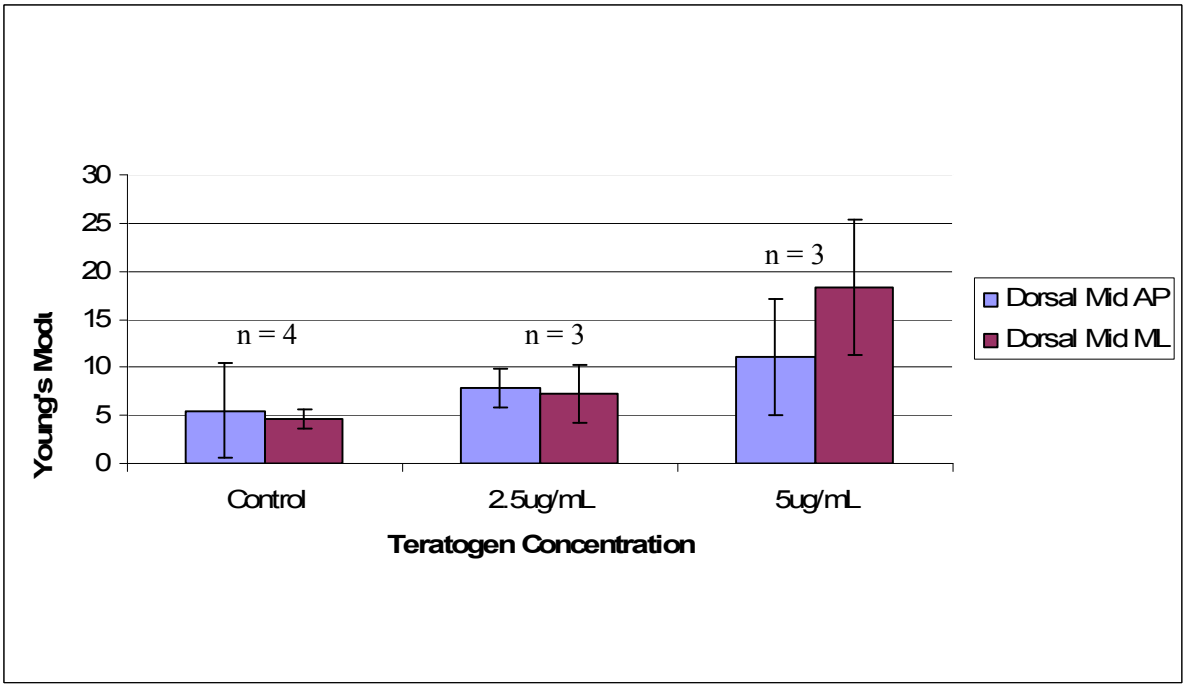

Figure 3.5 Shows correlation between cytochalasin B concentration and tensile properties of mid-dorsal tissue. An increase in Resultant Young's Modulus post drug treatment is observed.

Table 5 Correlation between cytochalasin B concentration and tensile properties of mid-lateral tissue

Stretch Direction	Anterior-Posterior			Medio-Lateral		
Drug Concentration	Control n = 4	2.5ug/mL n = 3	5ug/mL n = 3	Control n = 4	2.5ug/mL n = 3	5ug/mL n = 3
Resultant Young's Modulus N/m	10.9	7.03	11.8	4.58	11.3	5.6
Standard Deviation	+/-2.5	+/-5.1	+/-0.51	+/-1.3	+/-7	+/-1.7
Percentage Change	--	-35.5%	+8.25%	--	+146.74%	+22.2%

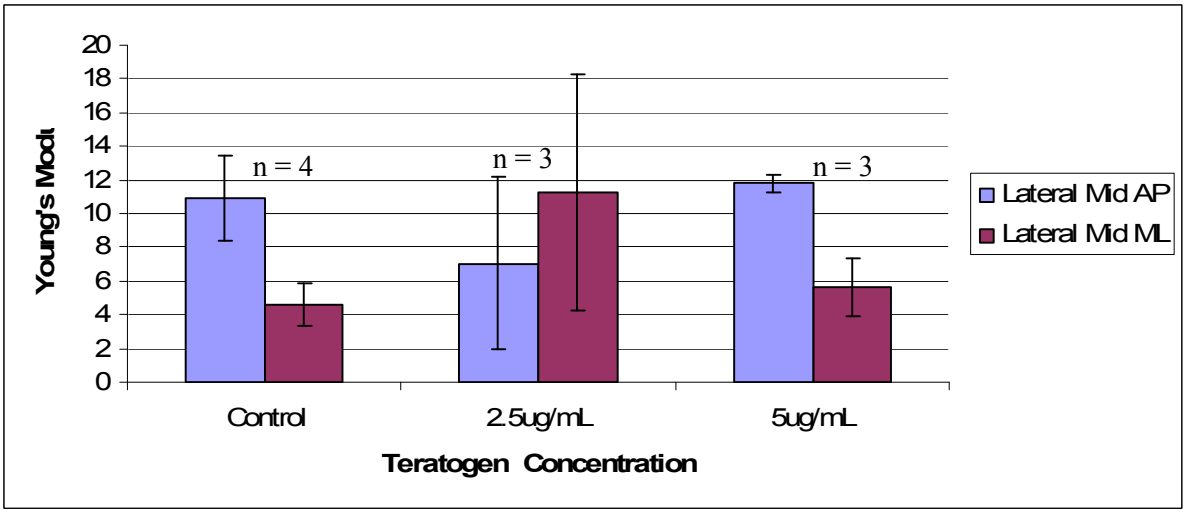

Figure 3.6 Correlation of cytochalasin B concentration and tensile properties of mid-lateral tissue. Variation in the change in Resultant Young's Modulus is seen based on the direction the tissue is stretched.

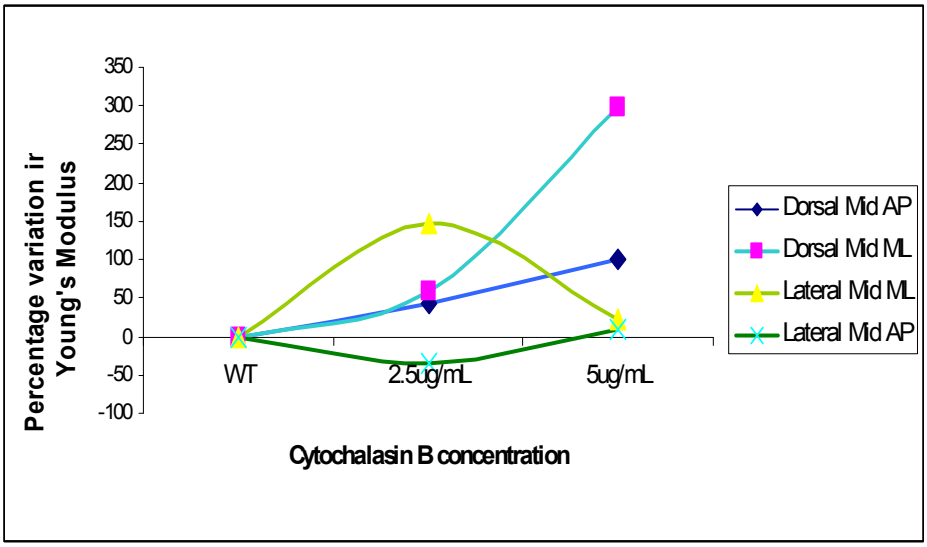

Figure 3.7 Percentage change in the Resultant Young's Modulus of normal tissue versus cytochalasin B treated tissue. The green lines depict the lateral tissue while the square and kite depict the dorsal region. The light lines depict tissue stretched in the medio-lateral direction while the dark lines depict tissue stretched in the anterior-posterior direction. The dorsal mid region shows an increase in stiffness while the lateral mid tissue depends on stretch direction

3.3.2 Effect of Cytochalasin B on Development

Cytochalasin B affects all stages of development. Externally applied cytochalasin B has been used to block gastrulation movements in *Xenopus* embryos (Bluemink, 1978). The three embryonic germ layers; ectoderm, endoderm, and mesoderm react differently to cytochalasin B treatment. Extensive damage to endoderm and mesoderm is required in order to halt the process of gastulation. Up to the gastrula stage, *Xenopus* embryos do not dissociate in the presence of low but effective doses of 5ug/mL cytochalasin B unless mechanical damage to the embryonic surface has occurred (Bluemink, 1978). Due to these reasons, embryos were treated at stage 13, post-gastrulation in order to determine the morphological affect on neurulating embryos.

The effect of cytochalasin B on embryo development was determined by comparing the teratogen treated embryo with control embryos. Figure 3.8 shows a control stage 15 embryo. The neural ridges as well as the neural anlage can be seen clearly. Stage 15 is the beginning of neural tube formation. The posterior region closes before the anterior region and the first contact between the neural ridges is at the mid-plate. While the control embryo reaches stage 15, the 2.5ug/mL

cytochalasin B treated embryo is stationary at stage 13 (Figure 3.9A). The neural cleft or the neural ridges cannot be observed. However the shape of the embryo is maintained and the dorsal region is easily differentiated from the lateral and ventral regions. Upon washing the 2.5ug/mL CB-treated embryo is able to resume normal development. Embryos treated with 5ug/mL of cytochalasin B show sever neural defects (Figure 3.9B). These embryos exhibit anencephaly where the anterior neural tube does not close properly.

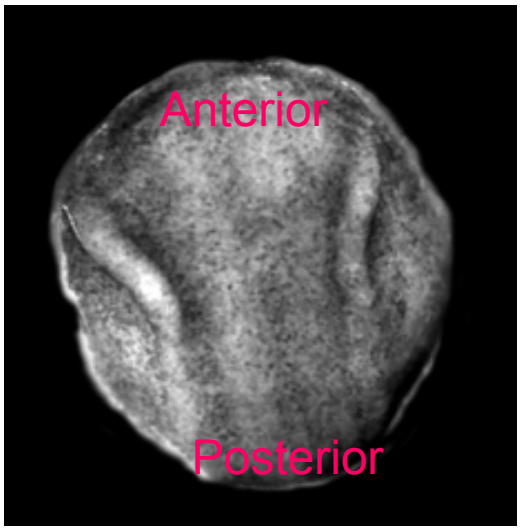

Figure 3.8 Control embryo at stage 15. The neural ridges and the neural plate can be clearly seen. Top of the picture is the anterior region and bottom is the posterior region. Picture is taken from the dorsal angle.

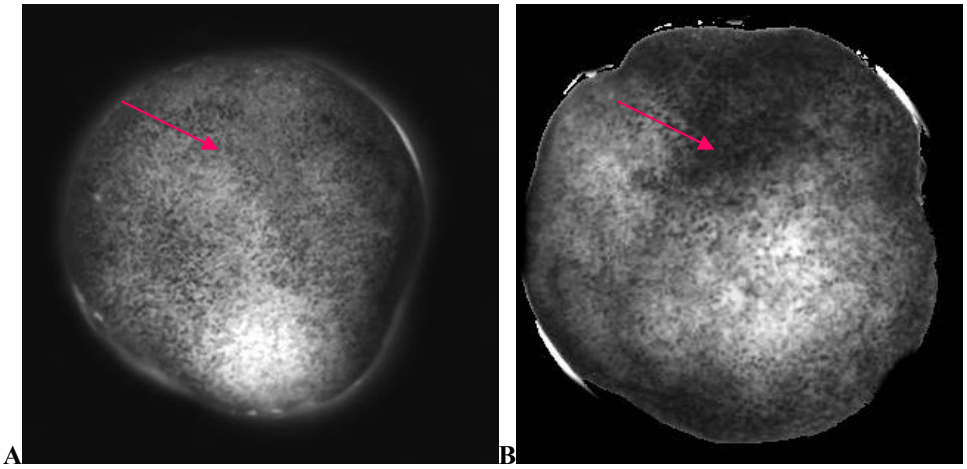

Figure 3.9 A.Embryo treated with 2.5ug/mL of cytochalasin B at stage 15. Developmental retardation is observed. B Embryo treated with 5ug/mL of cytochalasin B at stage 15. Severe phenotypic defects can be observed.

3.3.3 Effect of Cytochalasin B on Phalloidin Staining

The teratogen treated embryos were fixed in 4% paraformaldehyde once the control embryos reached stage 15. Uniform microscopic settings were used to view all the images in order to obtain the most accurate comparison between the control and the teratogen treated embryos. Staining and viewing was concentrated on the neural anlage and the lateral epidermal tissue. Our staining shows that most of the F-actin was localized around the cell membrane and at the cell junctions. In some instances F-actin is also seen in the cytoplasm. We expect a decrease in fluorescent intensity once the embryos have been treated with the teratogen since CB inhibits F-actin polymerization. Figure 3.10 illustrates a control embryo at stage 15. The strongest staining is in the neural plate region. Embryos treated with 2.5 ug/mL of cytochalasin B show a stark decrease in fluorescent intensity (Figure 3.11). Similarly embryos treated with 5ug/mL of cytochalasin B do not show a decrease in fluorescent intensity (Figure 3.12) especially the 3X magnification of the neural fragment (image D). Errors in treatment caused by washing the embryo can be attributed to the discrepancy observed in fluorescence intensity. Reversibly bound CB could have easily dissociated upon washing. The shape of individual cells in the 5ug/mL treated tissue is polygonal compared to the much rounded control cells.

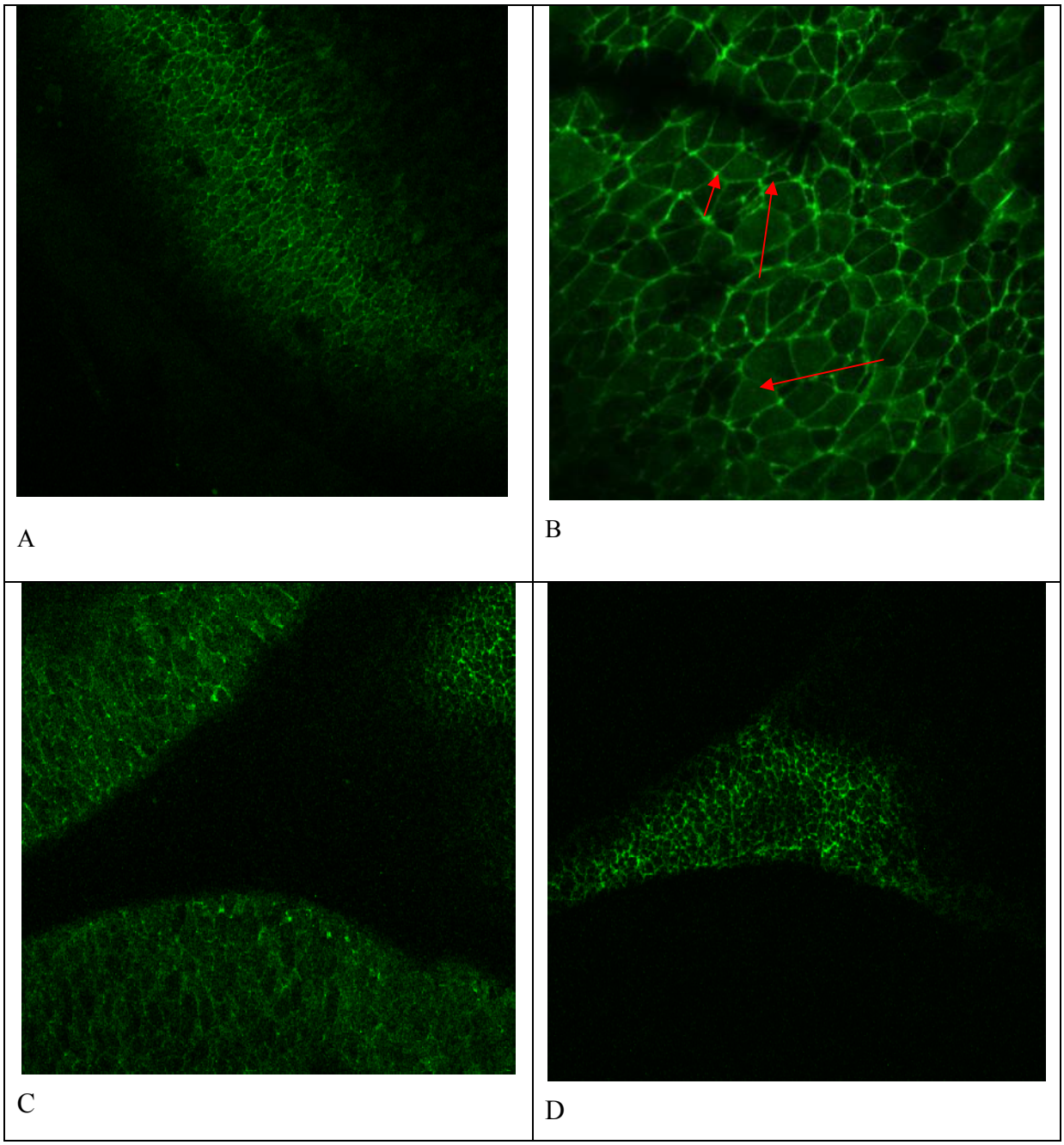

Figure 3.10 Control embryos stained with Phalloidin Alexa 488 to visualize presence of F-actin. Embryos were viewed under a confocal microscope A; Lateral section of a neurulating embryo. B; 3X magnification of A. The short arrow shows the cell junction, the medium arrow shows the cell membrane and the long arrow shows the cytoplasm. C; Lateral tissue close to the neural ridge. D; Neural Plate

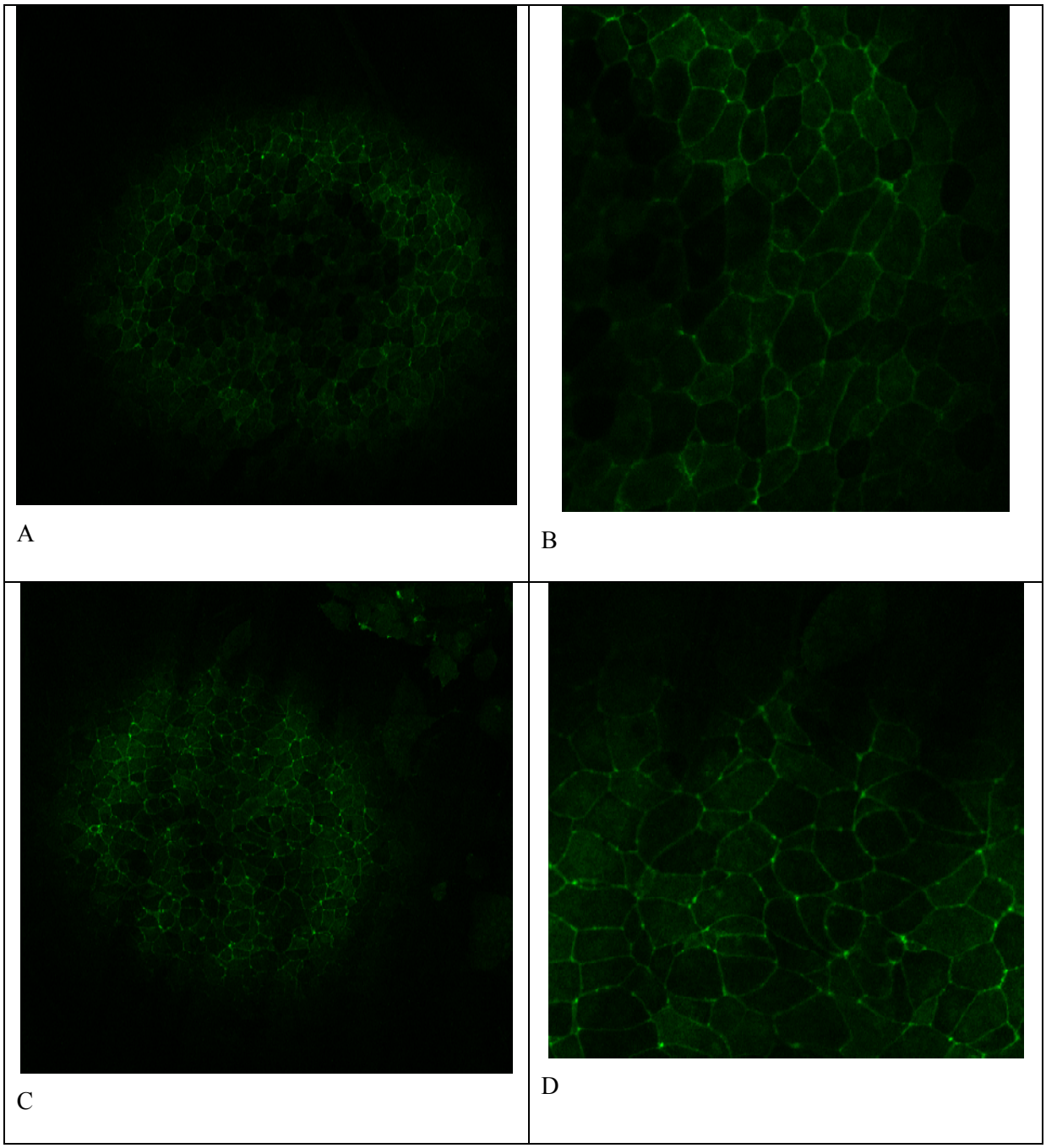

Figure 3.11 Sections of embryos treated with 2.5ug/mL of cytochalasin B. A; Lateral fragment of the embryo. B; 3X magnification of A. C; Neural fragment of the embryo D; 3X magnification of C.

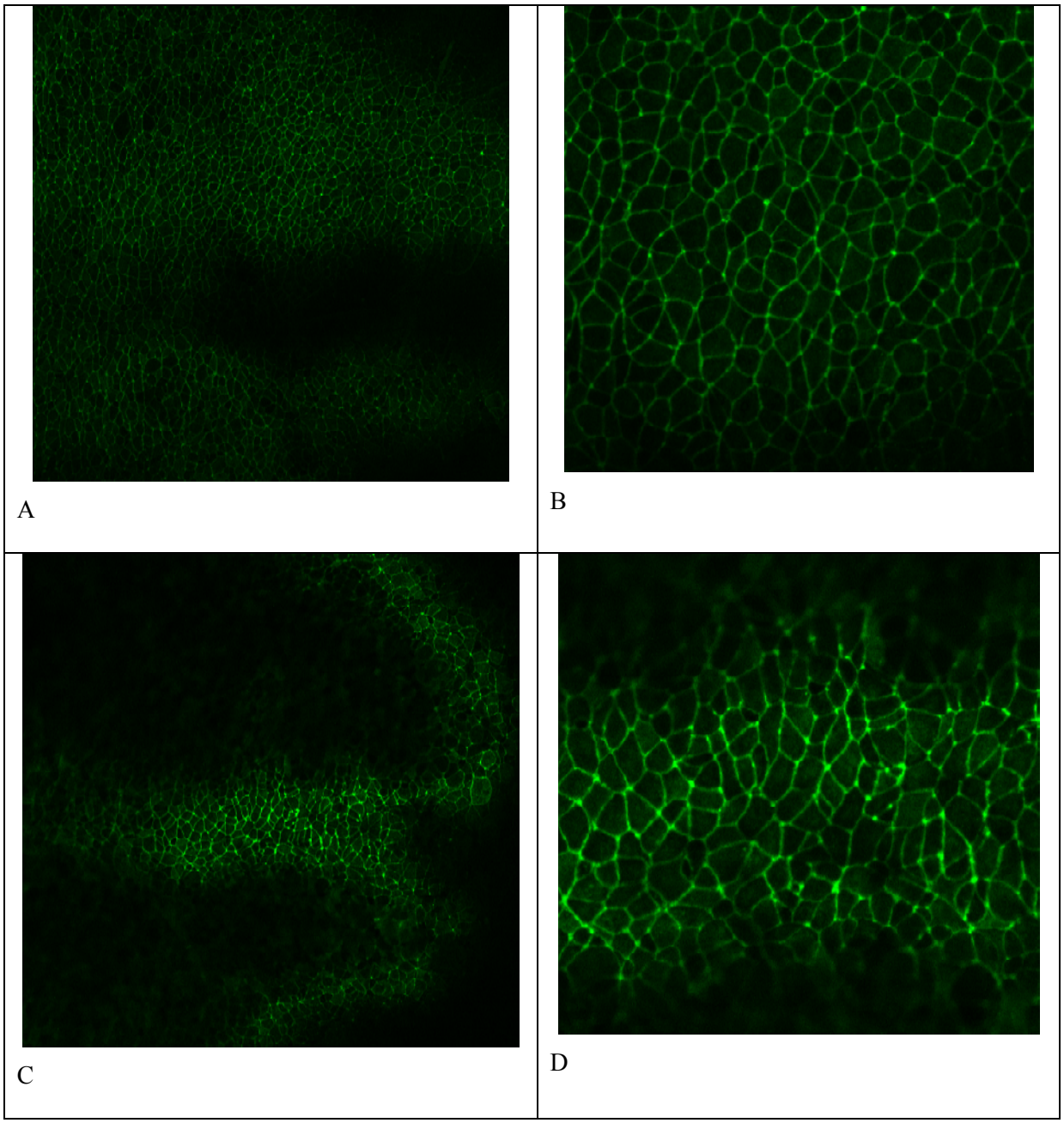

Figure 3.12 Embryos treated with 5ug/mL of cytochalasin B. A; Lateral fragment close to the neural plate. B; 3X magnification of A. C. Neural fragment of the same embryo. D. 3X magnification of C.

3.3.4 Effect of Valproic Acid on Mechanical Properties

Stage 15 axolotl embryos were stretched in the medio-lateral and anterior-posterior direction at 5mM concentration of valproic acid. The dorsal-mid and lateral-mid region of the axolotl embryo was investigated. The following table summarizes the Resultant Young's Modulus of control compared to teratogen treated tissue. Figure 3.13 shows that embryos treated with valproic acid portray a prominent increase in tissue stiffness.

Table 6 Correlation between Resultant Young's Modulus of valproic Acid (5mM) treated mid-dorsal and mid-ventral tissue stretched in AP and ML direction

Stretch Direction	Anterior-Posterior				Medio-Lateral			
Tissue Location	Mid-Dorsal		Mid-Lateral		Mid-Dorsal		Mid-Lateral	
Drug Concentration	Control n = 4	Valproic Acid (5mM) n = 3	Control n = 4	Valproic Acid (5mM) n = 3	Control n = 4	Valproic Acid (5mM) n = 3	Control n = 4	Valproic Acid (5mM) n = 3
Resultant Young's Modulus	5.53	20.9	10.9	13.9	4.6	19.3	4.58	8.07
Standard Deviation	5	16	2.5	6.94	1	2.22	1.3	6.71
Percentage Change	--	+277.9	--	+27.5	--	+319.5	--	+76.2

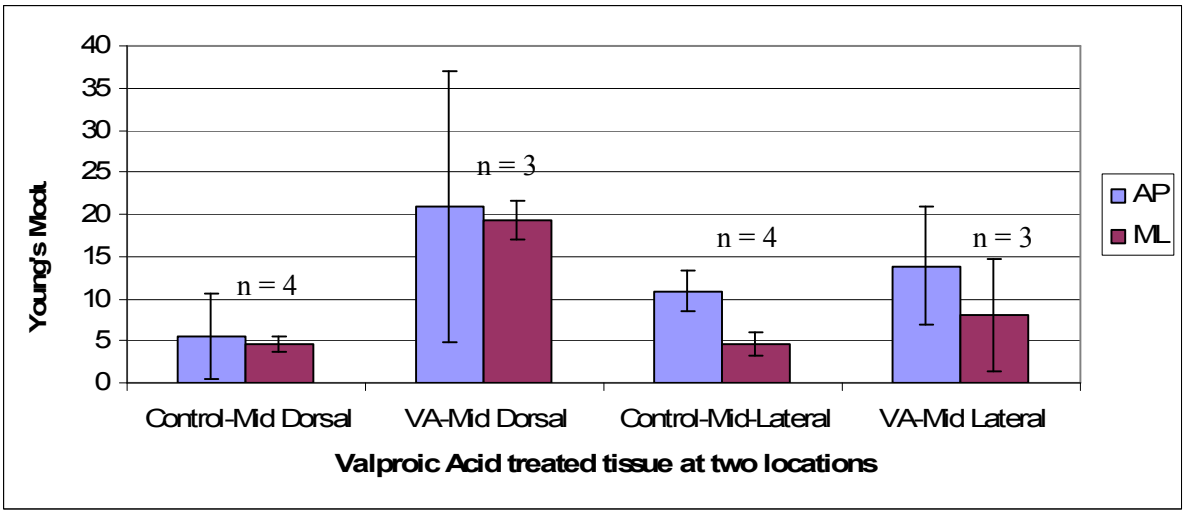

Figure 3.13 Correlation between teratogen treated tissue excised from mid-dorsal and mid-lateral region stretched in the anterior-posterior and medio-lateral direction. A greater increase in the Resultant Young's Modulus is seen when the tissue is stretched in the mid-dorsal region as opposed to the mid-lateral region.

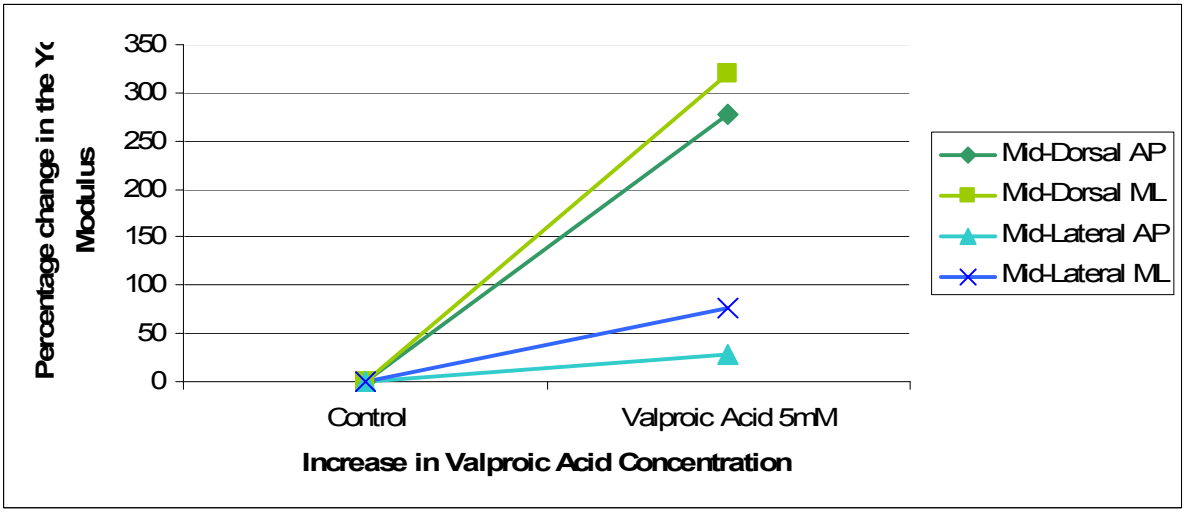

Figure 3.14 Percentage change in the Resultant Young's Modulus of valproic Acid treated tissue with respect to normal tissue. Each line represents a different tissue sample stretched in the anterior-posterior and medio-lateral direction

3.3.5 Effect of Valproic Acid on Development

Figure 3.16 shows an axolotl embryo treated with 5mM of valproic acid dissolved in 1% Steinberg's solution. Control embryos were at stage 15 when the picture Figure 3.15 was taken. VA treated embryos showed retarded development and wavy neural folds. Some embryos showed edema (figure not shown).

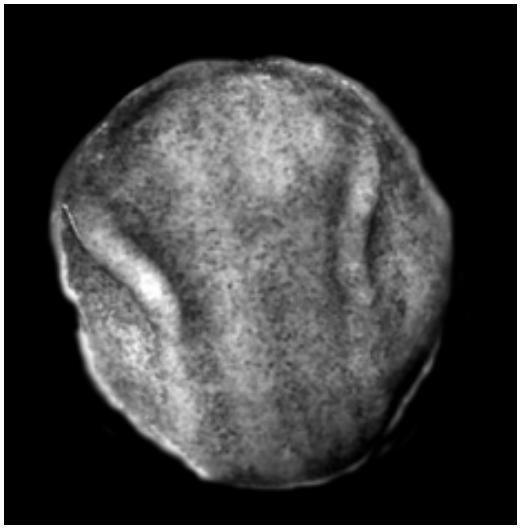

Figure 3.15 Shows the control embryo at stage 15

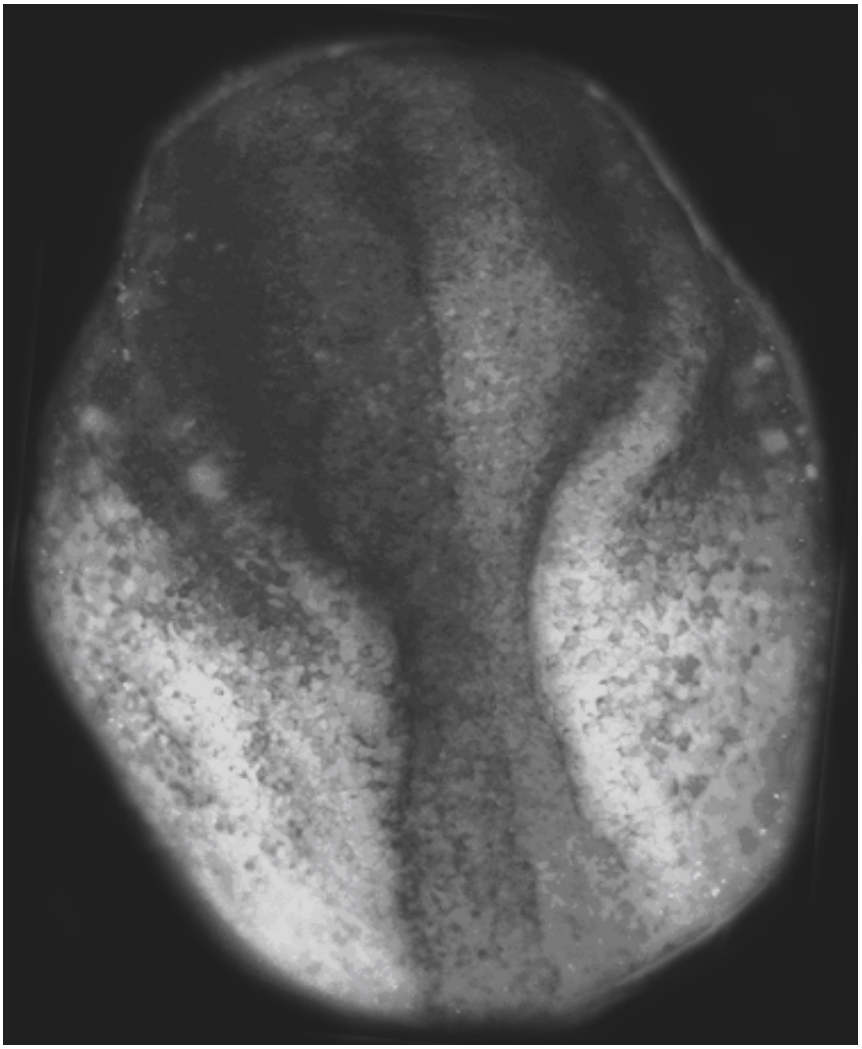

Figure 3.16 Valproic acid treated axolotl embryo when the control embryo reaches stage 15. Embryos exhibits enencephaly.

3.3.6 Effect of Valproic Acid on Phalloidin Staining

Figure 3.16, shows VA treated axolotl tissue stained with phalloidin. An increase in phalloidin intensity is observed compared to the control sections. Phalloidin intensity has been localized to the cell membrane and cell junctions. The phalloidin-stained samples are consistent with our expectation that Valproic acid causes an increase in F-actin filaments.

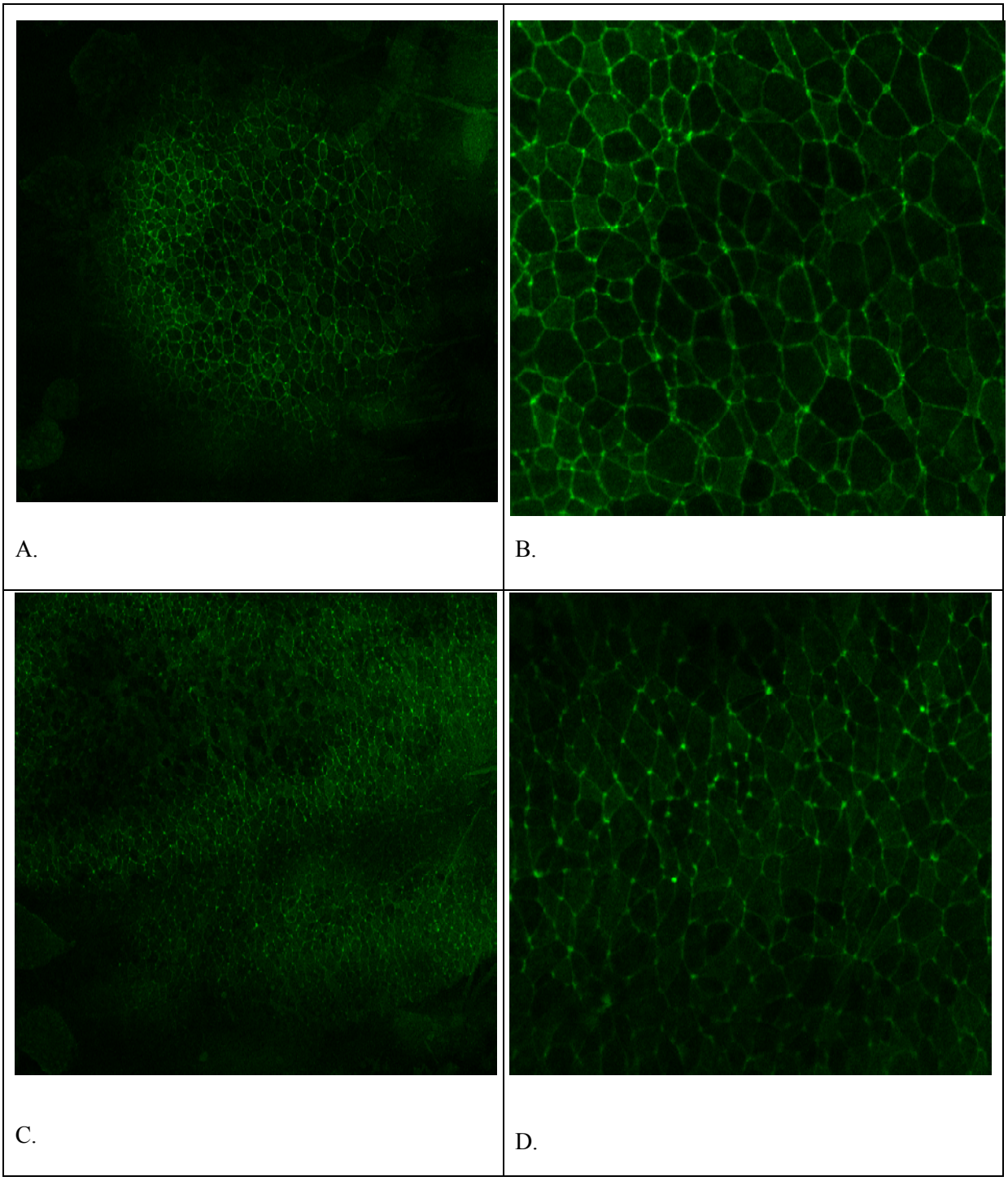

Figure 3.17 Embryos treated with 5mM valproic acid. A; Lateral fragment of a drug treated embryo. B; X3 magnification of A. C; Neural Fragments of axolotl embryos. D; 3X magnification of C.

3.3.7 Statistical Analysis

Chi-square testing was performed in order to obtain the statistical significance of our results. The expected value for the four different treatments (control, 2.5ug/mL CB, 5ug/mL CB and 5mM VA) was calculated from the average of all the values. Table below summarizes the expected value, actual value and P-value for all the results.

Table 7 Shows the expected values and P-values for all the tests conducted.

Test Parameter	Values	Control n = 4	2.5ug/mLCB n = 3	5ug/mL CB n = 3	5mM VA n = 3	P-value
Dorsal-Mid AP	Expected	11.37	11.37	11.37	11.37	
	Actual	5.53	7.98	11.1	20.9	0.00726
Dorsal-Mid ML	Expected	12.38	12.38	12.38	12.38	
	Actual	4.6	7.32	18.3	19.3	0.000103
Lateral-Mid AP	Expected	10.9	10.9	10.9	10.9	
	Actual	10.9	7.03	11.8	13.9	0.518
Lateral-Mid ML	Expected	7.39	7.39	7.39	7.39	
	Actual	4.58	11.3	5.6	8.07	0.304

A p-value of < 0.005 suggests that the dorsal mid section gave a statistically significant result. We are able to state with 95% confidence that the teratogens caused an effect on the dorsal mid section of our tissue when stretched in the AP and ML direction. However the > 0.05 p-value of the mid-lateral section suggests that the mechanical alterations are random and that the drugs did not cause an effect on the ventral section.

Chapter 4: Discussion

This thesis focuses on identifying the correlation between teratogen treatment, alterations in cytoskeleton structure, and changes in tissue mechanical properties. Figure 4.1 below summarizes the multi-step process.

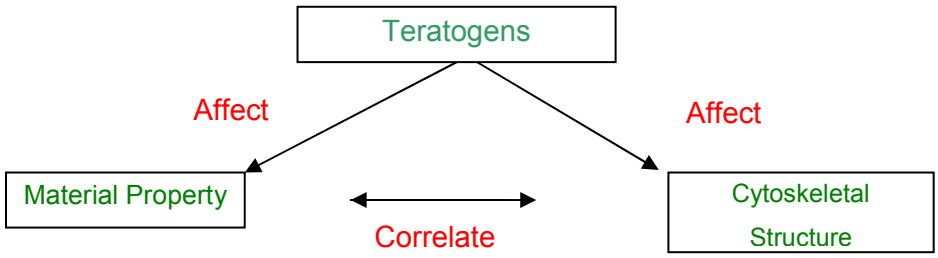

Figure 4.1 The correlation between cytoskeletal structures and material properties

Cytochalasin B inhibition of F-actin polymerization affects all stages of development. Externally applied cytochalasin B has been used to block gastrulation movements in *Xenopus* embryos (Bluemink, 1978). The three embryonic germ layers; ectoderm, endoderm, and mesoderm react differently to cytochalasin B treatment. Up to the gastrula stage, *Xenopus* embryos do not show a phenotype in the presence of low but effective doses of 5ug/mL cytochalasin B unless mechanical damage to the embryonic surface has occurred (Bluemink, 1978). Due to these reasons, embryos were treated at stage 13, post-gastrulation in order to determine the morphological affect on neurulating embryos. Two different concentrations were used to determine the optimal drug concentration. An optimal drug concentration is high enough to have a strong affect on the embryo yet weak enough to ensure the embryo survives. The lower drug concentration, 2.5ug/mL delayed development. However, if the embryo was allowed to grow after washing, it was able to resume regular developmental activity. The 5ug/mL concentration of cytochalasin B caused serious developmental defects. The embryo shrivelled up, suggesting a strong affect of cytochalasin B on the tissue integrity. Cytochalasin B is known to alter the shape of the cells (Bluemink, 1978). Cells start to disaggregate near the neural folds. Perhaps cells along the neural folds and hinge points are under higher mechanical stress thus preventing the neural tube from closing as a consequence of cytochalasin B

treatment. The embryo also exhibited spina bifida, where the neural tube does not close at the posterior end.

Valproic acid (VA) is a known human teratogen causing neural tube defects, spina bifida aperta and anencephaly in 1-2% of human foetuses exposed to the compound during early pregnancy (Walmod et al., 1999). VA is also responsible for causing cardiovascular, urogenital, and craniofacial abnormalities in human foetuses (Kratke and Kirschbaum, 1996). Valproic acid strongly disturbs the cellular integrity of the neuroepithelium. In VA treated axolotls disorganized neural epithelium, incomplete bending and perturbed neural fold fusion is observed. Affects of VA on the cytoskeletal structures also affects the morphology of neural development. Increased intracellular spaces and reduced cell adhesion was attributed to VA treatment in a study conducted by Kratke and Kirschbaum (1996). Valproic acid did not have any effect on the ectodermal cells and the differentiation and elongation of the notochord. However, VA affected mesodermal structures in the axolotl embryo. To study the effect of excessive actin polymerization on neural development and tissue integrity 5mM valproic acid was used. Valproic acid-treated embryos exhibit anencephaly, failure of the anterior tube to close. The ectodermal tissue appeared rigid and strong however the underlying mesoderm cells appeared flaccid. Similar to cytochalasin B, valproic acid treated embryos were not able to close their neural tube properly perhaps due to mechanical stresses along the neural folds and lateral hinge points caused by increased tissue-stiffness in that area.

Fifty-one axolotl embryos (stage 15) were stretched in two different directions; AP and ML. The tissue studied was excised from the mid-dorsal neural anlage and mid-lateral epidermis. Control tissue was than compared to two different teratogen treated tissues; cytochalasin B and valproic acid. Cytochalasin B disrupts actin polymerization and a decrease in actin concentration was observed. Contrary to cytochalasin B, valproic acid prevents actin from depolymerizing and an increase in the actin concentration was observed when stained with phalloidin. The table below summarizes the values of the Resultant Young's Moduli obtained from all the tests. An overall increase in tissue stiffness is observed in the teratogen treated tissue compared to the control tissue.

Table 8 Summary of the Resultant Young's Modulus (N/m) measured from neurulating axolotl tissue

Stretch Direction	Anterior-Posterior				Medio-Lateral			
Location	Control n = 4	2.5ug/mL n = 3	5ug/mL n = 3	Val(5mM) n = 3	Control n = 4	2.5ug/mL n = 3	5ug/mL n = 3	Val(5mM) n = 3
Mid-Dorsal	5.5	7.93	11.1	20.9	4.6	7.2	18.3	19.3
Mid-Lateral	10.9	7	11.8	13.9	4.6	11.3	5.6	8.07

The mid-dorsal neural anlage was found to be isotropic since the control embryos gave similar Young's Modulus of ~5N/m when stretched in either direction. The mid-dorsal section tested with 2.5 ug/mL of CB showed a similar trend of 50% increase, when stretched in either direction. This shows that the increase in the tissue stiffness caused by the 2.5ug/mL sample acted in a direction independent manner. However, the 5ug/mL concentration of the drug caused the Resultant Young's Modulus to increase by 100.7% and 289% when stretched in the AP and ML direction respectively. These values suggest that the 5ug/mL CB causes the neural anlage to exhibit anisotropy. The valproic acid treated tissue gave a huge increase of ~300% when stretched in either direction as expected since VA is known to induce actin polymerization. The huge increase means that the microfilaments play a prominent role in the dorsal anlage since VA prevents actin depolymerization. The value increase by the same amount confirms the fact that the dorsal tissue exhibits uniform microfilament alignment that can exert equal stress in either direction, rendering the tissue to be isotropic. Furthermore VA causes an increase in tissue stiffness, but does not alter the microfilament orientation.

The mid-lateral epidermal tissue showed strong dependence on the direction the tissue was stretched. Control tissue provided a value of 11N/m when stretched along the AP direction and 5N/m when stretched along the ML direction. This suggests that the mid-lateral tissue was anisotropic. When stretched in either direction, the 5ug/mL CB treated tissue gave a similar Young's Modulus to the control. This simply means that the microfilaments do not provide significant structural support in the epidermal tissue or that the 5ug/mL CB did not have a strong affect on the microfilament

polymerization. This is supported by the phalloidin stain samples of control embryos exhibiting the same fluorescence as the 5ug/mL CB samples. The 2.5ug/mL CB treated tissue gave a 35.5% decrease when stretched along the AP direction; as expected by the phalloidin-stained samples where a decrease in fluorescence is observed compared to the control samples and since the microfilaments could be oriented along the AP direction. The only exception to the observed trend is the mid lateral tissue stretched in the AP direction when treated with 2.5ug/mL of cytochalasin B. Tissue stretched in the ML direction increased the Resultant Young's Modulus by 146.7% for the 2.5ug/mL CB. This suggests that the 2.5ug/mL CB may have caused the tissue to change its stiffness in a direction dependent fashion as explained by the decrease in the AP-stretch direction and increase in the ML-stretch direction. VA treated tissue increased by 27.5 % and 76.2% when stretched in the AP and ML direction respectively. This reaffirms the fact that VA increases microfilament polymerization and tissue stiffness, VA does not alter the microfilament orientation, and that the MF could be oriented along the AP direction as opposed to the ML direction.

Phalloidin strongly binds to filamentous F-actin; strong stain intensity suggests a high concentration of polymerized F-actin. The tissue samples were fixed prior to phalloidin treatment preventing phalloidin from affecting F-actin polymerization. Stained samples show a higher intensity near the cell-cell junctions and cell membranes. This demonstrates that F-actin is found near the cell boundary thereby playing a positive role in cell movement and migration. Our results illustrate the highest phalloidin intensity in the valproic acid treated samples, confirming that valproic acid increased F-actin polymerization. The 2.5ug/mL cytochalasin B-treated samples showed a decrease in phalloidin staining while the 5ug/mL CB-treated sample gave the same intensity as the control. The cells in the 5ug/mL CB-treated tissue gave a more polygonal shape compared to the controls. The cell boundary appeared clearer and defined while the control cell boundary seemed fuzzier. Absence of microfilaments could induce interfacial tension on the cell boundary therefore causing the cell membrane to appear rigid.

We expected the Resultant Young's Modulus to decrease as the concentration of cytochalasin B increased. However, except for the mid-lateral tissue stretched in the mediolateral direction, the Resultant Young's Modulus for all the teratogen treated tests increased. We can deduce that the drug may have induced a negative feedback mechanism that could have increased the concentration of another protein in the cells thereby contributing to the tissue stiffness. Another plausible explanation regarding the increase in tissue stiffness due to inhibition of actin polymerization stems from a recent

study conducted by Drees et al. (2005) on α-catenin activity. Their results show that α-catenin does not bind simultaneously to the cadherin-catenin complex and actin filaments. The interaction of α-catenin with actin filaments significantly decreases the affinity of α-catenin for the E-cadherin-β-catenin complex (Yamada et al., 2005). Decreased actin filament could result in α-catenin binding to the cadherin-catenin complex, therefore increasing cell-cell contacts and increasing the integrity of the tissue.

According to Wiebe and Brodland (2004), when the specimen was elongated to a true strain of 0.15 the load increased approximately linearly with an initial slope or Resultant Young's Modulus E (given in units of N/m since the thickness of the tissue was not taken into account). The experiment was ceased as soon as the tissue started to tear and a true strain of approximately 0.48 N/m was revealed once the tearing became evident. As the tissue tore, the load dropped dramatically to approximately 20% its peak value. The ectoderm was detached from mesoderm thus the stress measured was not influenced by lower layers and the force in the tissue was specific to the neural ectoderm. This study provides an accurate comparison of the forces in the epidermis and the neuroepithelium of a normal embryo with that of teratogen treated embryos.

The increased stiffness of the mid-dorsal neural anlage along the mediolateral axis could be due to increased cell-cell or cell-matrix adhesion, increased stiffness of the cytoskeleton, increased stiffness of the extracellular matrix, or some combination of these. Since the changes observed are caused due to cytoskeleton-affecting teratogens, therefore the variations in the Resultant Young's Moduli must reflect mechanical properties of the cytoskeleton rather than adhesion. This does not imply that adhesion is not important in tissue mechanics, or that adhesion does not change but that adhesion is not the source of the increase in the Resultant Young's Modulus. Adhesion is important to allow cell intercalation and to preserve tissue integrity (Moore et al., 1995). These results are in agreement with Moore et al., (1995), who proposed that the cytoskeleton is supported by proteins resisting tension parallel to the mediolateral axis of the embryo as convergent extension begins.

One of the fundamental reason cytochalasin B and valproic acid were used, besides causing microfilament alterations, was that these drugs caused severe neural tube defects in axolotls that strongly resemble neural tube defects in humans, such as spina bifida and anencephaly. Spina bifida

and anencephaly are birth defects found in humans caused by a variety of reasons. The results of this research will help provide a greater understanding of neural tube birth defects.

4.1 Sources of Error

It is important to note that teratogens such as cytochalasin B and valproic acid are broad drugs that affect a variety of proteins and biochemical processes in the developing embryo. It is possible that these drugs may have influenced other aspects of neurulation that may cause a discrepancy in the results. Furthermore, since the embryos were washed before testing, cytochalasin B, which binds reversible to actin filament, may have been washed out as well.

The error in measuring forces using the tissue tester was a combination of the accuracy of calibration, size measurements, software imaging and wire tracking. The stress resultants are the amount of force per unit of tissue width rather than stresses and are reported because the epithelium is not uniform across its thickness due to differences between the neural plate and the epidermal ectoderm. Right after the embryos were glued to the wires, the tissue between was excised from the rest of the embryo. The vitelline membrane was removed prior to the gluing process and was assumed not to have any affects on neurulation.

Underlying mesoderm cells may perhaps influence the forces measured. The mesoderm of stage 15 embryo was loosely attached to the mid dorsal section, thereby rendering calculations in that region to be accurate and consistent. However, the mid lateral epidermis comprised a tightly bound lining of mesoderm layer that was pried out using an eye-lash tool. This non-automated process by which the mesoderm was removed may have caused discrepancy in the results due to residual cells in the lateral section. Efforts were made to ensure that the neural ridges were clearly removed, however residual neural ridges left in the dorsal section could perhaps cause a discrepancy in the results.

4.2 Future Work

Future studies could look at measuring tissues in additional regions, like the anterior and posterior neural anlage and ventral sections. It would also be beneficial to measure axolotl embryos at different stages of development. Lastly, testing for other cytoskeletal structures like microtubules and selectively blocking expression of membrane proteins would give a good estimate of the impact of these proteins on tissue integrity. Last but not least, a device that is able to measure biaxial tissue stretching would prove to be beneficial in providing information on the anisotropic nature of the neural epithelial.

4.3 Conclusions

Our tests show that the dorsal region is more susceptible to the drug treatment giving a 300% increase in the Young's Modulus while the lateral tissue was found to be a lot more resistant to the drug treatment giving a maximum increase of 100.7% due to the teratogen treatment. The lateral tissue forms the presumptive epidermal layers. It is differentiated from the neural tissue by the presence of E-cadherins instead of N-cadherins. These drug-induced changes in material properties appear to be sufficient to explain the abnormal phenotypes the drugs produce.

Appendix A

Table 9 Shows the true stress and the true strain during the first 1500 seconds

Time (seconds)	True Strain	True Stress (N/m)
0	0	0
30	0.000110	5.52E-05
60	0.000120	8.31E-05
90	0.000256	0.000103
120	0.000345	0.000132
150	0.000499	0.000154
180	0.000674	0.000181
210	0.002103	0.000202
240	0.005665	0.000243
270	0.003534	0.000273
300	0.010814	0.00031
330	0.007425	0.000347
360	0.008909	0.000387
390	0.008579	0.000425
420	0.011749	0.000468
450	0.012287	0.000513
480	0.015582	0.000557
510	0.01938	0.000606
540	0.020933	0.000647
570	0.025203	0.000697
600	0.026684	0.000731
630	0.02796	0.000775
660	0.028179	0.000809
690	0.03162	0.000849
720	0.035666	0.000881

750	0.040007	0.000922
780	0.040231	0.00095
810	0.04338	0.000989
840	0.044471	0.001019
870	0.047071	0.001063
900	0.051475	0.001111
930	0.053841	0.001153
960	0.054567	0.001187
990	0.056427	0.001233
1020	0.057742	0.001271
1050	0.059662	0.001313
1080	0.05625	0.001345
1110	0.063816	0.001396
1140	0.066401	0.00144
1170	0.065694	0.001479
1200	0.069671	0.001524
1230	0.071889	0.001559
1260	0.072746	0.001602
1290	0.076905	0.001648
1320	0.078646	0.001699
1350	0.081011	0.001753
1380	0.083651	0.001804
1410	0.085494	0.001855
1440	0.087433	0.001904
1470	0.087324	0.001954
1500	0.093859	0.002008

Appendix B

Test Parameters for each experiment

Stretch Direction	Experiment #	Wire Length (mm)	Image Scale (pixels/mm)
DOR_MID_CT			
AP	1	64	440
AP1	10	66	440
AP3	14	62	546
AP5	58	61	440
ML	5	60	440
ML 1	9	66	440
ML 2	12	66	440
ML3	13	62	440
ML4	59	60	686
DOR_MID_2.5CB			
AP	11	66	546
AP1	21	74	546
AP2	26	61	546
AP3	27	61	546
ML	4	60	440
ML1	6	66	440
ML2	28	61	440
ML3	30	64	440
DOR_MID_5.0CB			
AP	3	64	546
AP1	7	66	440
AP2	8	66	440
ML	2	64	546
ML1	18	58	440
ML2	19	58	440
LAT_MID_CT			
AP	15	58	546

AP1	16	58	546
AP2	33	64	546
AP3	60	56	686
ML	17	58	440
ML1	25	64	440
ML2	31	64	440
ML3	32	64	440
ML4	61	56	440
LAT_MID_2.5CB			
AP	20	74	546
AP1	29	61	546
AP2	34	62	546
AP3	35	63	546
ML	22	74	440
ML1	36	63	546
ML2	40	65	546
ML3	41	65	546
ML4	42	64	546
LAT_MID_5.0CB			
AP	26	64	440
AP1	37	63	546
AP2	39	65	686
ML	23	64	440
ML1	24	64	440
ML2	38	63	440
DOR_MID_VAL			
AP	43	64	546
AP1	45	60	546
AP2	47	60	546
AP3	53	60	546
ML	44	64	440

ML1	54	60	440
ML2	55	61	440
LAT_MID_VAL			
AP	48	62	546
AP1	49	62	546
AP2	52	65	546
ML	46	60	440
ML1	50	62	440
ML2	51	65	546
ML3	56	61	440
ML4	57	61	440

Appendix C

Table 10 Value of Resultant Young's Modulus from all the tests performed. CT = control, CB = cytochalasin B, VA = valproic acid, AP = anterior-posterior direction, ML = medio-lateral direction

Name	Test1	Test2	Test3	Test4	Average Test Value	Standard Deviation
CT-Mid Dorsal-AP	3.8	10.9	24.3	-	5.53	+/-5
CT-Mid Lateral-AP	9.3	9.1	14.5	10.8	10.9	+/-2.5
CT-Mid Dorsal-ML	5.5	5.1	3.2	18.9	4.6	+/-1
CT-Mid Lateral-ML	3.4	3.6	6.0	5.3	4.58	+/-1.3
CB2.5-Mid Dorsal-AP	6.8	6.9	10.1	-	7.93	+/-2
CB2.5-Mid Lateral-AP	1.9	7.1	12.1	-	7.03	+/-5.1
CB2.5-Mid Dorsal-ML	4.0	9.8	7.9	-	7.32	+/-3
CB2.5-Mid Lateral-ML	9.6	20.7	4.0	10.7	11.3	+/-7
CB5-Mid Dorsal-AP	13.8	4.6	14.8	-	11.1	+/-6
CB5-Mid Lateral-AP	11.7	12.4	11.4	-	11.8	+/-0.51
CB5-Mid Dorsal-ML	11.1	18.9	24.9	-	18.3	+/-7
CB5-Mid Lateral-ML	6.7	6.5	3.6	-	5.6	+/-1.7
VA5mM-Mid Dorsal-AP	38.6	7.3	16.8	-	20.9	+/-16
VA5mM -Mid Lateral-AP	10.7	9.2	21.9	-	13.9	+/-7
VA5mM -Mid Dorsal-ML	18.1	18.0	21.9	-	19.3	+/-2.2
VA5mM –Mid Lateral-ML	9.1	0.9	14.2	-	8.07	+/-6.7

Appendix D

Appendix D shows the graphs of the values obtained in the fifty-one tests conducted.

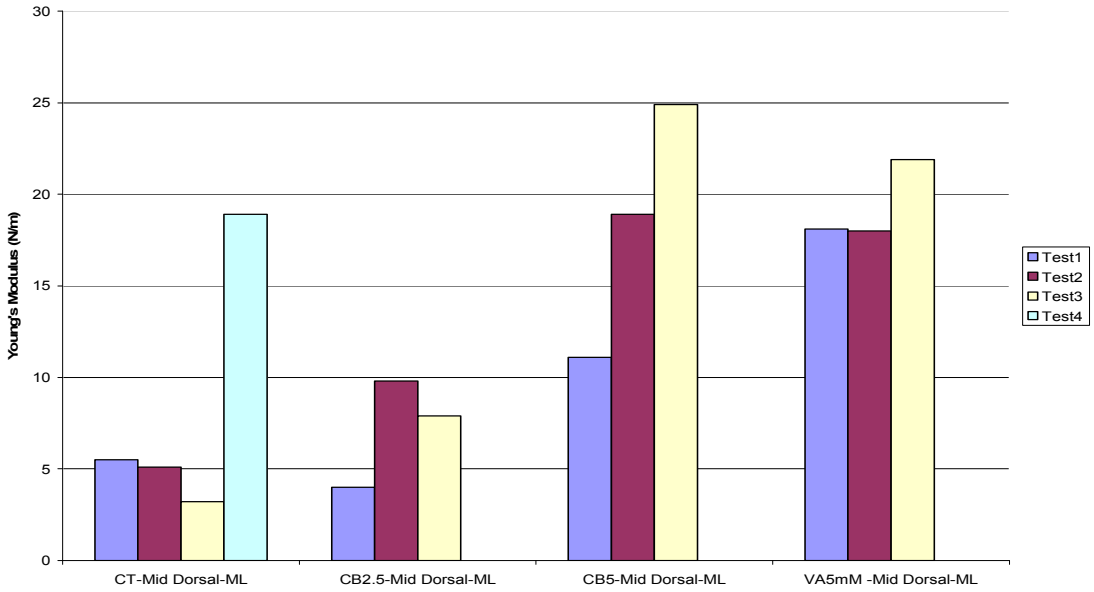

Figure 4.2 Shows the value of the Resultant Young's Modulus obtained from the mid-dorsal tissue stretched in the medio-lateral direction.

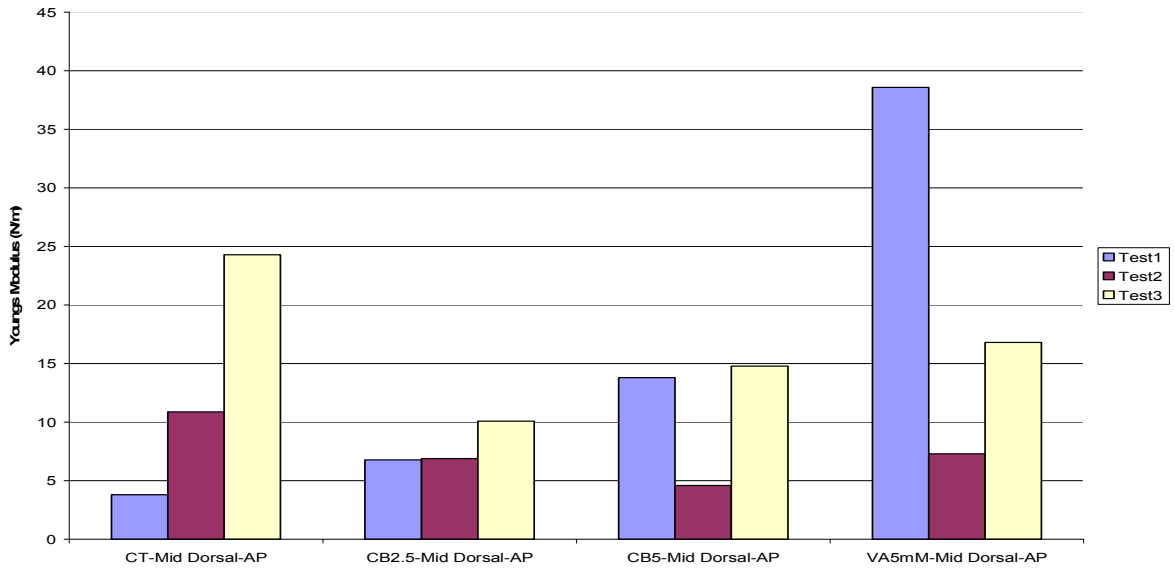

Figure 4.3 Shows the value of the Resultant Young's Modulus obtained from the mid-dorsal tissue stretched in the anterior-posterior direction.

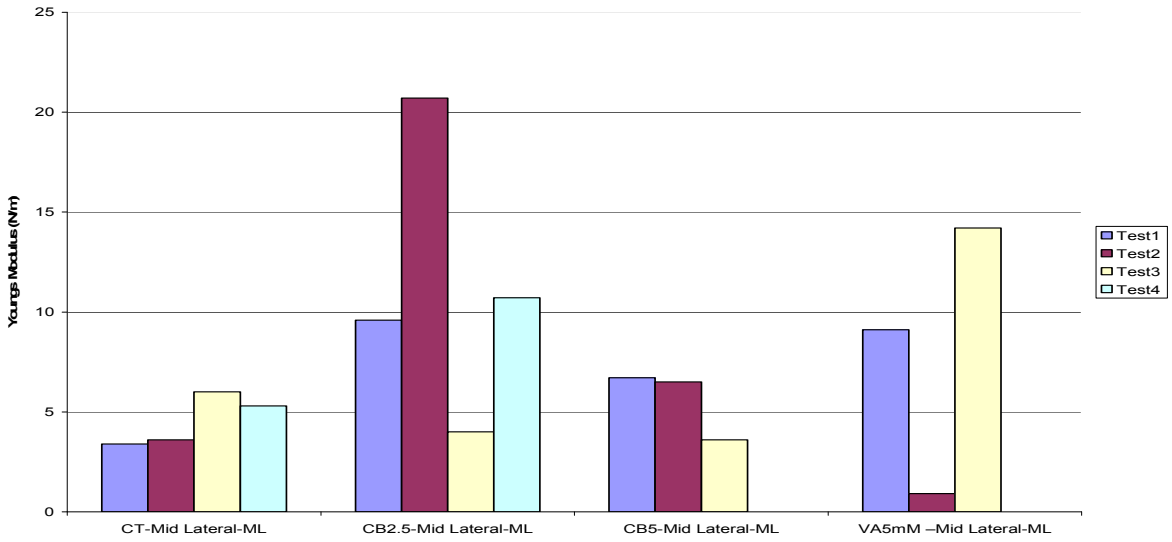

Figure 4.4 Shows the value of the Resultant Young's Modulus obtained from the mid-lateral tissue stretched in the medio-lateral direction.

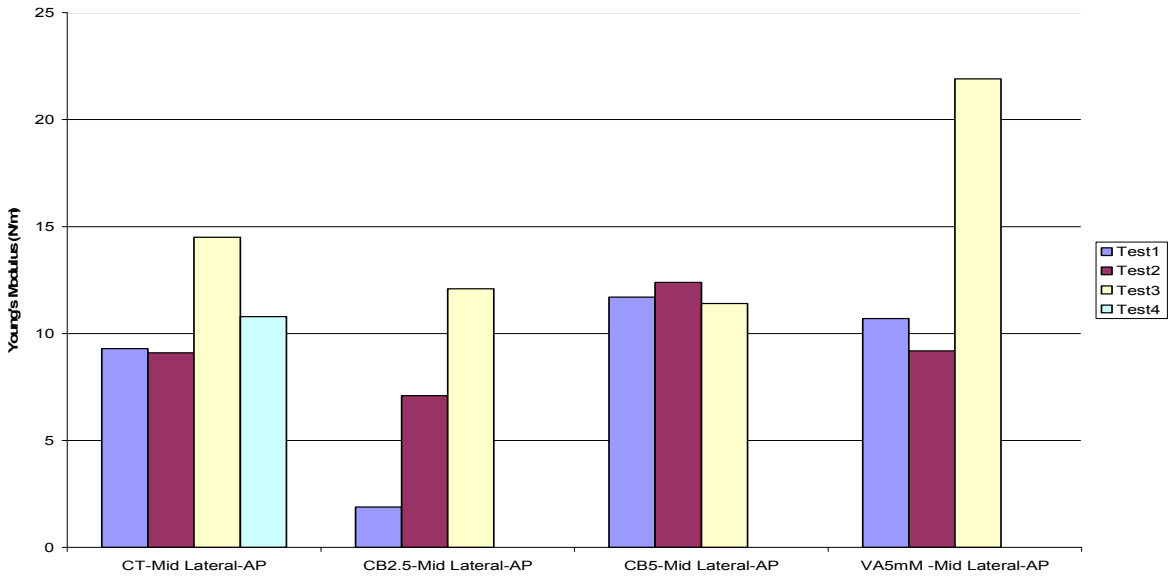

Figure 4.5 Shows the value of the Resultant Young's Modulus obtained from the mid-lateral tissue stretched in the medio-lateral direction.

Bibliography

1. Adams, A. E., & Pringle, J. R. (1991). Staining of actin with fluorochrome-conjugated phalloidin. *Methods in enzymology, 194*, 729-731.
2. Berezin, V., Kawa, A., Bojic, U., Foley, A., Nau, N., Regan, C., Edvardsen, K., & Bock, E. (1996). Teratogenic Potency of Valproate Analogues evaluated by Quantitative Estimation of Cellular Morphology. *In Vitro. Toxicol In Vitro 10,* 585-94.
3. Bluemink, J. G. (1971) Effects of Cytochalasin B on surface contractility and cell junction formation during cleavage in *Xenopus laevis*. *Cytobiologie, 3,* 176-187.
4. Bluemink, J. G. (1978) Use of Cytochalasins in the study of amphibian development. In *Cytochalasins: Biochemical and cell biological aspects* edited by S. W. Tanenbaum. Elsevier/North-Holland Biomedical Press, New York, pp. 113-142.
5. Bordzilovskaya, N. P., T. A. Dettlaff, Susan, T. Duhon, & Malacinski. 1989. Developmental-stage series of axolotl embryos. In *Developmental Biology of the Axolotl* edited by J. B. Armstrong and G. M. Malacinski. Oxford University Press, New York, pp. 201-219.
6. Brodland, G. W. (2003). New information from cell aggregate compression tests and its implications for theories of cell sorting. *Biorheology, 40(1-3),* 273-277.
7. Brodland, G. W., Gorson, R., Scott, M. J., Bjorklunk, N. K., Luchka, K. B., Martin, C. C., Matuga, C., Globus, M., Vethamany-Globus, S., & Shu, D. (1994). Furrowing surface contraction wave coincident with primary neural induction in amphibian embryos. *Journal of morphology, 219*(2), 131-42.
8. Brun, R. B., & Garson, J. A. (1983). Neurulation in the mexican salamander (ambystoma mexicanum): A drug study and cell shape analysis of the epidermis and the neural plate. *Journal of embryology and experimental morphology, 74*(0), 275-295.
9. Brun, R. B., & Garson, J. A. (1984). Notochord formation in the Mexican Salamander (*Ambystoma mexicanum)* is different from the notochord formation in *Xenopus laevis. The journal of experimental zoology, 229*(2), 235-240.

10. Burnside, B. (1971). Microtubules and Microfilaments in newt neuralation. *Developmental biology, 26*(3), 416-441.
11. Burnside, B. (1973) Microtubules and Microfilaments in amphibian neurulation, *Amer. Zool., 13,* 989-1006.
12. Burnside, B., & Jacobson, A. G. (1968). Analysis of morphogenetic movements in the neural plate of the Newt Taricha toroso. *Developmental biology, 18*(0), 537-552.
13. Burnside, B., & Manasek, F. J. (1972). Cytochalasin B: Problems in interpretating its effect on cells. *Developmental biology, 27*(3), 443-444.
14. Chou, K. Y., & Els, W. J. (1995). Distribution of actin microfilaments in frog skin epithelial granular cells. *Biology of the cell / under the auspices of the European Cell Biology Organization, 83*(1), 61-68.
15. Clausi, D. A., & Brodland, G. W. (1993). Mechanical evaluation of theories of neurulation using computer simulations. *Development, 118,* 1013-1023.
16. Cooper, J. A. (1987). Effects of Cytochalasin and Phalloidin on actin *J. Cell Biol, 105, 1*473-1478.
17. Copp, A. J. (1994). Genetic models of mammalian neural tube defects. In *Neural Tube Defects* edited by G. Bock and J. Marsh. John Wiley & Sons Ltd., England, pp. 118-143.
18. Copp, A. J., & Brook, F. A. (1989). Does lumbosacral spina bifida arise by failure of neural folding or by defective canalization? *J. of Medical Genetics, 26,* 160-166.
19. Desai, A., & Mitchison, T. J. (1997). Microtubule polymerization dynamics. *Annual Review of Cell and Developmental Biology, 13*(0), 83-117.
20. Detrick, R. J., Dickey, D., & Kinter, C. R. (1990). The effect of N-cadherin misexpression on morphogenesis in *Xenopus* embryos. *Neuron, 4,* 493-506.
21. Drees, F., Pokutta, S., Yamada, S., Nelson, W. J., & Weis, W. I. (2005). Alpha-catenin is a molecular switch that binds E-cadherin-beta-catenin and regulates actin-filament assembly. *Cell, 123*(5), 903-915.

22. Duprat, A. M. (1996). What mechanisms drive neural induction and neural determination in urodeles? *Int. J. Dev. Biol., 40,* 745-754.
23. Fankhauser, G., & Humphrey, R. R. (1952). The rare occurrence of mitosis without spindle apparatus ("colchicine mitosis") producing endopolyploidy in embryos of the axolotl. *Proceedings of the National Academy of Sciences of the United States of America, 38*(12), 1073-1082.
24. Gallera, J. (1971). Primary induction in birds. *Advances in Morphogenesis, 9*(0)*,* 148-180
25. Gilbert, S. F. (2003). Later Embryonic Development, In *Developmental Biology, Seventh Edition*. Sinauer Associates Inc., Sunderland, pp. 314-360.
26. Gont, L. K., Steinbeisser, H., Blumberg, B., & de Robertis, E. M. (1993). Tail formation as a continuation of gastrulation: The multiple cell populations of the xenopus tailbud derive from the late blastopore lip. *Development (Cambridge, England), 119*(4), 991-1004.
27. Gordon, R. (1085). A review of the theories of vertebrate neurulation and their relationship to the mechanics of neural tube birth defects. *J. of exp. Morph. 89*(Supplement), 229-255.
28. His, W. (1874) Our body form and the physiological problem if its development, Letters to a friendly naturalist, Unsere Körperform und das physiologische Problem ihrer Entstehung. F. C. W. Vogel, Leipzig.
29. Haigo, S. L., Hildebrand, J. D., Harland, R. M., & Wallingford, J. B. (2003). Shroom induces apical constriction and is required for hingepoint formation during neural tube closure. *Current biology : CB, 13*(24), 2125-2137.
30. Handel, M. A., & Roth, L. E. (1971). Cell shape and morphology of the neural tube: Implications for microtubule function. *Developmental biology, 25*(1), 78-95.
31. Jacobson, C. O. (1962). Cell migration in the neural plate and the process of neurulation in the axolotl larva. *Zool. Bidr. Upps. 35,* 433-449
32. Jacobson, C. O., & Lofberg, J. (1969) Mosiderm movements in the amphibian neurula. *Zool. Bidrag. Uppsala Bd 38*(17), 233-239.

33. Jacobson, C. O. (1981). Morphogenesis of the neural plate and tube. In *Morphogenesis and Pattern Formation* edited by T. G. Connelly. Raven Press, New York, pp. 233-263.

34. Jacobson, C. O. (1991). Experimental analysis of the shaping of the neural plate and tube. *Amer. Zool., 31*(0), 628-643.

35. Jacobson, C. O. (1994). Normal neurulation in amphibians. In *Neural Tube Defects* edited by G. Bock and J. Marsh. John Wiley & Sons Ltd., England, pp. 6-24.

36. Karfunkel, P. (1971). The role of microtubules and microfilaments in neurulation in xenopus. *Developmental biology, 25*(1), 30-56.

37. Karfunkel, P. (1974). The mechanisms of neural tube formation. *International review of cytology, 38*(0), 245-271.

38. Keller, R. (2002). Shaping the vertebrate body plan by polarized embryonic cell movements. *Science, 298,* 1950-1955.

39. Keller, R., Shih, J., Sater, A. K., & Moreno, C. (1992). Planar induction of convergence and extension of the neural plate by the organizer of *Xenopus*. *Developmental dynamics : an official publication of the American Association of Anatomists, 193*(3), 218-234.

40. Kratke, R., & Kirschbaum, F. (1996). Effects of the antiepileptic drug valproic acid on the development of the axolotl (ambystoma mexicanum): Histological investigations. *Teratogenesis, carcinogenesis, and mutagenesis, 16*(3), 149-167.

41. Lewis, W. H. (1947). Mechanics of invagination. *Anat. Rec., 97,* 139-156.

42. Lin, S., & Spudich, J. A. (1974). On the molecular basis of action of cytochalasin B. *Journal of Supramolecular Struc. 2,* 728-736.

43. Molecular Probes, (2007). Fluorophores and their amine-reactive derivatives. In *The Handbook- A Guide to Fluorescent Probes and Labeling Technologies, 10th Edition.*

44. Moore, S. W., Keller, R. E., & Koehl, A. R. (1995). The dorsal involuting marginal zone stiffens anisotropically during its convergent extension in the gastrula of *Xenopus levis. Developmental, 121,* 3131-3140.

45. Nieuwkoop, P. D. (1999). The neural induction process; its morphogenetic aspects. *The International journal of developmental biology, 43*(7), 615-623.

46. Oberemm, A., & Kirschbaum, F. (1992). Valproic acid induced abnormal development of the central nervous system of three species of amphibians: Implications for neural tube defects and alternative experimental systems. *Teratogenesis, carcinogenesis, and mutagenesis, 12*(6), 251-262.

47. Papalopulu, N., & Kintner, C. R. (1994). Molecular genetics of neurulation. In *Neural Tube Defects* edited by G. Bock and J. Marsh. John Wiley & Sons Ltd., England, pp. 90-102.

48. Puszkin, E., Puszkin, S, Lo, L. W., & Tanenbaum, S. W. (1973). Binding of cytochalasin D to platelet and muscle myosin. *J. of Biochem. 248,* 7754-7761.

49. Schoenwolf, G. C. (1994) Formation and patterning of the avian neuroaxis: One dozen hypotheses. In *Neural Tube Defects* edited by G. Bock and J. Marsh. John Wiley & Sons Ltd., England, pp. 25-50.

50. Schoenwolf, G. C., & Smith, J. L. (1990). Mechanism of neurulation: Traditional viewpoint and recent advances. *Development, 109,* 234-270.

51. Schroeder, T. E. (1970). Neurulation in xenopus laevis. an analysis and model based upon light and electron microscopy. *Journal of embryology and experimental morphology, 23*(2), 427-462.

52. Schroeder, T. E. (1971). Mechanisms of morphogenesis: The embryonic neural tube. *The International journal of neuroscience, 2*(4), 183-197.

53. Schrorder, T. E. (1973). Cell constriction: Contractile role of microfilaments in division and development. *Amer. Zool., 13,* 949-960.

54. Small, J. V., Stradal, T., Vignal, E., & Rottner, K. (2002). The lamellipodium: Where motility begins. *Trends in cell biology, 12*(3), 112-120.

55. Spudich, J. A., &Lin, S. (1971). Cytochalasin B, its interaction with actin and actomyosin from muscle. *Proc. Nat. Acad. Sci. USA, 69*(2), 442-446

56. Tannenbaum, J., Tannenbaum, S. W., & Goodman, G. C. (1975). Binding and subcellular location of tritiated Cytochalasin D. *Exp. Cell Res.,91,* 47-56

57. Tannenbaum, J. (1978). Approaches to the molecular biology of Cytochalasin action. In *Cytochalasins: Biochemical and cell biological aspects* edited by S. W. Tanenbaum. Elsevier/North-Holland Biomedical Press, New York, pp. 521-560.

58. Tamai, K., Yokota, C., Ariizumi, T., & Asashima, M. (1999). Cytochalasin B inhibits morphogenetic movement and muscle differentiation of activin-treated ectoderm in xenopus. *Development, growth & differentiation, 41*(1), 41-49.

59. Tamai, K., Yokota, C., Ariizumi, T., & Asashima, M. (1999). Cytochalasin B inhibits morphogenetic movement and muscle differentiation of activin-treated ectoderm in xenopus. *Development, growth & differentiation, 41*(1), 41-49.

60. van Straaten, H. W. M., & Coop, A. J. (2001). Curly tail: a 50-year history of the mouse spina bifida model. *Anat. Embryol. 203,* 225-237.

61. Wallingford, J. B., & Harland, R. M. (2001). Xenopus dishevelled signalling regulates both neural and mesodermal convergent extension: parallel forces elongating the body axis. *Development, 128(13),* 2581-2592.

62. Walmod, P. S., Skladchikova, G., Kawa, A., Berezin, V., & Bock, E. (1999). Antiepileptic teratogen valproic acid (VPA) modulates organisation and dynamics of the actin cytoskeleton. *Cell motility and the cytoskeleton, 42*(3), 241-255.

63. Weihing, R. R. (1976) Cytochalasin B inhibits actin-related gelation of HeLa cell extracts. *The Journal of Cell Biology, 71,* 303-307.

64. Wiebe, C. J. (2003). A micro-scale tensile tester for embryonic epithelia. The University of Waterloo, Waterloo, pp. 34-44.

65. Wiebe, C., & Brodland, G. (2004). Tensile properties of embryonic epithelia measured using a novel instrument. *Journal of Biomechanics, 38*(10), 208-2094.

66. Yamada, S., Pokutta, S., Drees, F., Weis, W. I., & Nelson, W. J. (2005). Deconstructing the cadherin-catenin-actin complex. *Cell, 123*(5), 889-901.